BIOMETRIC IDENTIFICATION THROUGH HAND VEIN PATTERNS

by

Aycan Yüksel

B.S, Computer Engineering, Kocaeli University, 2007

Submitted to the Institute for Graduate Studies in
Science and Engineering in partial fulfillment of
the requirements for the degree of
Master of Science

Graduate Program in Computer Engineering

Boğaziçi University

2010

BIOMETRIC IDENTIFICATION THROUGH HAND VEIN PATTERNS

APPROVED BY:

Prof. Lale Akarun (Thesis Supervisor)	.....
Prof. Bülent Sankur (Thesis Co-supervisor)	.....
Assoc. Prof. Burak Acar	.....
Assist. Prof. A. Taylan Cemgil	.....
Dr. Hülya Yalçın	.....

DATE OF APPROVAL: 21.06.2010

ACKNOWLEDGEMENTS

I would like to express my deepest gratitude to my thesis supervisor Lale Akarun for her insight, endless patience and stimulation that I needed to complete this work. I would like to thank my cosuperi Prof. Bulent Sankur for his continuous discussions, clever ideas on the topic. Without their supervision and efforts, this work may not have seen the light of day.

I thank the PILAB members and all my other friends and teachers in the department for their support.

The greatest thanks is to my family for their encouragement, endless support and trust. I am specifically grateful to Muharrem Demir, who believed in me with boundless patience throughout this thesis.

ABSTRACT

BIOMETRIC IDENTIFICATION THROUGH HAND VEIN PATTERNS

Many biometric systems, such as face, fingerprint and iris have been studied extensively for personal verification and identification purposes. Biometric identification with vein patterns is a more recent approach that uses the vast network of blood vessels underneath a person's skin. These patterns in the hands are assumed to be unique to each individual and they do not change over time except in size. As veins are under the skin and have a wealth of differentiating features, an attempt to copy an identity is extremely difficult. These properties of uniqueness, stability and strong immunity to forgery of the vein patterns make it a potentially good biometric trait which offers greater security and reliable features for personal identification. In this thesis, we present a novel hand vein database and a biometric technique based on the statistical processing of the hand vein patterns. The hand vein database has been collected under realistic conditions in that subjects had to undergo the procedures of holding a bag, pressing an elastic ball and cooling with ice, all exercises that force changes in the vein patterns. The applied recognition techniques are a combination of geometric and appearance-based techniques and good identification performances have been obtained on the database.

ÖZET

EL DAMAR ÖRÜNTÜLERİYLE BİYOMETRİK TANIMA

Yüz tanıma, iris tanıma ve parmak izi tanıma gibi birçok biyometrik sistem, kimlik tanıma ve doğrulama amacıyla yaygın bir şekilde çalışılmıştır. Deri altındaki damar ağını kullanan, damar örüntüleriyle biyometrik tanıma, yeni bir yaklaşımdır. Eldeki bu örünütülerin kişiye özgü olduğu ve büyüklükleri haricinde değişmediği sanılmaktadır. Damarlar, deri altında gözlemlendikleri ve zengin ayırtedici özelliklere sahip olduklarından, bir kimliği kopyalama girişimi son derece zordur. Teklik, değişmezlik ve taklit edilemezlik gibi özelliklerinden dolayı damar örüntüleri güvenilir ve inandırıcı bir biyometrik tanıma adayıdır. Bu tezde, el damar örüntülerinin istatistiksel işlenmesine dayalı bir biyometri tekniği sunulmuştur. El damar veritabanı, kullanıcıların çanta taşıma, elastik bir topu sıkma, eli buz ile soğutma gibi damar örüntülerini değişmeye zorlayan işlemlere tabi tutulduğu gerçekçi koşullar altında toplanmıştır. Tanıma için şekil bilgisi ve görünüme dayalı yöntemlerin karışımı kullanılmıştır ve veritabanı üzerinde umut vaad edici sonuçlar elde edilmiştir.

TABLE OF CONTENTS

LIST OF FIGURES

LIST OF TABLES

LIST OF SYMBOLS/ABBREVIATIONS

A	Images taken after opening and closing the fist (activity)
B	Images taken after carrying a bag (bag)
B_O	Background of original (ground-truth) image
B_T	Background of test image
d_θ	Angular distance
$d_\parallel$	Parallel distance
$d_\perp$	Perpendicular distance
F_O	Foreground of original (ground-truth) image
F_T	Foreground of test image
I	Images taken after having cooled the image (ice)
max	Maximum
min	Minimum
N	Images taken under normal condition (normal)
μm	micrometer
nm	nanometer
2D	Two Dimensional
3D	Three Dimensional
CCD	Charged Coupled Devices
EER	Equal Error Rate
FAR	False Accept Rate
FIR	Far Infrared Imaging
FRR	False Reject Rate
Hb	Hemoglobin
HD	Hausdorff Distance
ICA	Independent Component Analysis
ICA1	ICA Architecture I
ICA2	ICA Architecture II

IR	Infrared
LED	Light Emitting Diode
LEM	Line Edge Map
LHD	Line Segment Hausdorff Distance
LPP	Locality Preserving Projection
NIR	Near Infrared Imaging
NMF	Non-negative Matrix Factorization
PC	Personal Computer
PIN	Personal Identification Number
RBF	Radial Basis Function
RM	Reduced Multivariate
ROC	Receiver Operating Characteristics
ROI	Region of Interest
SVM	Support Vector Machine
TEST1	Results for Single Enrollment
TEST2	Results for Double Enrollment
TEST3	Results for 4× Enrollment
TEST4	Results for 8× Enrollment

1. INTRODUCTION

Various biometric techniques for personal identification such as face, fingerprint and iris images have been developed to make the systems more resistant to the problems of theft, loss, and reliance on the user's memory. In order to use a technique as biometric characteristic, it has to satisfy the requirements of universality, distinctiveness, permanence, collectability, performance, acceptability and circumvention [1]. In Table 1.1 comparison of various biometric technologies in terms of these requirements is given. Universality states that every individual should have the characteristic, distinctiveness states that the biometric data has to be unique to each individual, permanence measures how well a biometric resists aging and collectability measures how easy it is to acquire a biometric for measurement. Accuracy, speed, and robustness of the system is named as performance criteria. Circumvention defines how easy it is to fool the authentication system and lastly the acceptability indicates people's behaviour in terms of willingness to accept the use of the biometric characteristic.

Identification using vein patterns is less studied compared to other human traits probably because the vein pattern is not observable under visible light. The structure of the vein patterns can be detected and captured with the help of infrared sensors. The visibility of the vein structure depends on various factors such as age, thickness of the skin, ambient temperature, physical activity, and the imaged part of the hand. Surface features such as moles, warts, scars and hairs can also affect the quality of the images.

Vein pattern is the vast network of blood vessels underneath a person's skin. The shape of vascular patterns in the same part of the body is distinct from each other [2], and it is very stable over long periods, unaffected by aging, except in size. In addition, as the blood vessels are hidden underneath the skin and are invisible to the human eye, vein patterns are much harder to copy as compared to other biometric features.

1.1. Motivation

Developments in biometric technologies have achieved sufficiently high recognition rates under controlled conditions, but the need for reliability, robustness and convenience is still a major requirement that remains unfulfilled. Vein patterns appear as a good candidate for a user friendly interface, potentially reliable against elapsed time and changes in physical conditions. However, there are few studies regarding the repeatability, uniqueness of the actual vein pattern and considering the effects of temperature and physical activity. Furthermore, algorithm testing is usually carried out on a limited number of sample images acquired under different hardware setups due to the lack of open hand vein databases. Creating a large database of real hand vein patterns is a difficult task in terms of time and money. There are many papers that report good results but, none of these results are reproducible since the databases are not open. Thus, in this thesis we collect a hand vein database that is to be opened to researchers and we offer a novel implementation of different machine learning algorithms and their fusions on the collected hand vein database. The database has been collected from more than 100 individuals, by considering the effects of temperature and physical activity on hand veins.

1.2. Literature Review

There are two kinds of imaging technologies, namely Far-infrared (FIR) and Near-infrared (NIR) imaging. FIR technology that works within the range 8-14 μm is more suitable for capturing the large veins in the back of the hand, but it is sensitive to ambient conditions and does not provide a stable image quality. On the other hand, NIR imaging that works within the range 700-1000 nm produces good quality images when capturing vein patterns in the back of the hand, palm, and wrist. This band is more tolerant to changes in environmental and body conditions, but it also faces the problem of disruption due to skin features such as hairs and scars [5].

L. Wang *et al.* [5], proposed a person verification system using the thermal-imaged vein pattern in the back of the hand based on the Line Segment Hausdorff

Table 1.1. Comparison of various biometric technologies. High, medium and low are denoted by H, M, and L, respectively [1]

Biometric Identifier	Universality	Distinctiveness	Permanence	Collectability	Performance	Acceptability	Circumvention
DNA	H	H	H	L	H	L	L
Ear	M	M	H	M	M	H	M
Face	H	L	M	H	L	H	H
Facial thermogram	H	H	L	H	M	H	L
Fingerprint	M	H	H	M	H	M	M
Gait	M	L	L	H	L	H	M
Hand geometry	M	M	M	H	M	M	M
Hand vein	M	M	M	M	M	M	L
Iris	H	H	H	M	H	L	L
Keystroke	L	L	L	M	L	M	M
Odor	H	H	H	L	L	M	L
Palmprint	M	H	H	M	H	M	M
Retina	H	H	M	L	H	L	L
Signature	L	L	L	H	L	H	H
Voice	M	L	L	M	L	H	H

Table 1.2. Comparative survey of methods

Reference	Data	Methods and Results
		Verification
C.-L. Lin *et al.* [3],	32 users, 30 samples/subjects, total 960 images	Multi-resolution analysis. 5× enrollment. EER: 3.75
K. A. Toh *et al.* [4],	50 users, left and right hands, 10 samples/subjects, total 1000 images	Palm vein and palmprint scores are fused with SUM rule. SVM with RBF kernel is optimized for the vein features consisting of sub-sampled vein lines and for the directional wavelet energy features for palmprint. 5× enrollment.
L. Wang *et al.* [5],	30 users, 9 samples/subjects, total 270 images	Vein images are skeletonized as in [6] and LEM. Triple enrollment. EER is claimed to be 0.
		Identification
Y. Ding *et al.* [7],	48 users, 5 samples/subjects, total 240 images	The number of the end points and crossing points and the distances between them are used for feature extraction. Single enrollment. Identification rate: 99.1%.
Z. Wang *et al.* [8]	100 users, 5 samples/subjects, total 500 images	Single enrollment. Hausdorff, LEM and Gabor methods yield respectively 58%, 66% and 80%.
This thesis	100 users, 3 samples/user, 4 conditions, total 1200 images	ICA1, ICA2, LEM and NMF methods as well as their fusion are considered. Identification rates are 94.16% for single enrollment and 97.33% for double enrollment.

Distance (LHD). They reported correct recognition of all subjects in a database of 100 persons. In another paper, Z. Wang *et al.* [8] gave comparisons of shape and texture based methods for vein recognition. While shape similarity is measured via Hausdorff and Line Edge Map (LEM), texture similarity was measured via Euclidean distance of Gabor magnitude features. In a dataset of 100 persons, Hausdorff, LEM and Gabor based methods achieved an accuracy of 58%, 66%, 80%, respectively. They ended with a conclusion stating that Gabor based feature extraction get much better performance than traditional shape based methods since Gabor wavelet is robust to variation on gray-level images. C.-L. Lin *et al.* [3] present person verification results using palm dorsal images acquired from infrared (IR) images in the 3.4 - 5 μm band. Their approach is based on the combination of multiresolution images obtained from the pre-processed thermal vein images. G. Wang *et al.* [9] proposed a multimodal person identification system where palmprint and palm vein modalities were combined in a single image. Locality Preserving Projection (LPP) was used to extract features of the fused images and they called this "Laplacianpalm".

In [4], the authors collected 1000 NIR images, 10 images each from the right and left palm, from 50 different individuals. For feature extraction part, they investigated both palm vein and palm crease texture. For verification with palm vein, they first applied a Gaussian high pass filter. To enhance the edges of the vein structure, they applied morphological gradient operations such as erosion and dilation. Support Vector Machines (SVM) adopting different kernels (SVM-Linear, SVM-Poly, and SVM-RBF) and a Reduced Multivariate (RM) polynomial have been tested. SVM with RBF kernel and RM generalizes best for the two-fold experiments.

In [10], the watershed algorithm is directly applied to the gray-scale vein pattern images instead of gradient images and it is capable of locating the skeletons of the veins. The over-segmentation problem caused by watershed algorithm is solved by applying an opening operation followed by closing operation before applying the watershed method. The weaknesses of the algorithm are noted as merging close veins, missing thin veins and those that have floating endpoints.

In [7], the authors used a database of 240 instances, 5 images of one hand for 48 people. In this method, the segmentation effect has been improved from the single threshold to multi-thresholds. After applying median filtering, the image is thinned using a combination method of general conditional thinning and templates. The feature extraction is based on the end points and the crossing points. The distances between the end points and the distances between the crossing points have been calculated and the matching experiment is performed using these distances. A pass ratio of 99.1% has been noted for the approach. The weaknesses of the approach are speed problems in the segmentation part, the algorithm being simple and small sized database. A summary of the literature has been presented in Table 1.2.

1.3. Outline

The thesis is orginized as follows: Section 2 investigates the vein anatomy of the hand and the utilization of far and near-infrared imaging technologies for capturing veins in various parts of the hand. The imaging setup and the varialibities between the hand images captured during different times has been explained in a detailed way.

To verify the usefulness of the infrared hand vein images for biometrics, feature extraction techniques that use ICA, NMF and LEM methods and their fusion is proposed and implemented in Section 3.

In Section 4, the methodology for the experiments is reported and the experimental results are presented for identification and verification. Section 5 gives concluding remarks of the thesis and Section 6 future directions for the thesis and new methods are presented.

2. HAND VEIN STRUCTURE AND IMAGE ACQUISITION

New biometric applications based on physiological features have recently emerged, thanks to the use of different imaging technologies. These methods are used to study the content of biological pigments and tissue structures by analyzing the absorption and scattering of the induced light. The structure of the hand veins on the surface of the hand and image acquisition techniques for hand vein biometry will be discussed briefly in this chapter.

2.1. Hand Vein Anatomy

The most important physiological features that can be extracted from the back of the hand are the so called dorsal vein network. This is a network of veins formed by the dorsal metacarpal veins. There are mainly two types of hand veins found on the dorsum of the hand, namely cephalic and basilic. The basilic veins are the group of veins attached with surface of the hand and generally consist of upper limb of the back of hand. Cephalic veins are the group of veins attached with the elbow of the hand.

The veins of the human body extend or shrink with changes in the body. In general, no major growth takes place in adult life and hence vein patterns are quite stable in the age group of $20-50$. As the vascular system is a large and essential system of the body, it is largely affected due to any change in the body; either by nature or by disease. The diabetes, hypertension, atherosclerosis, metabolic disorders [11] and tumors [12] are some diseases which affect the vascular systems and either make it thick or thin. Figure 2.1 illustrates the generic vascular map found on the dorsum of the hand.

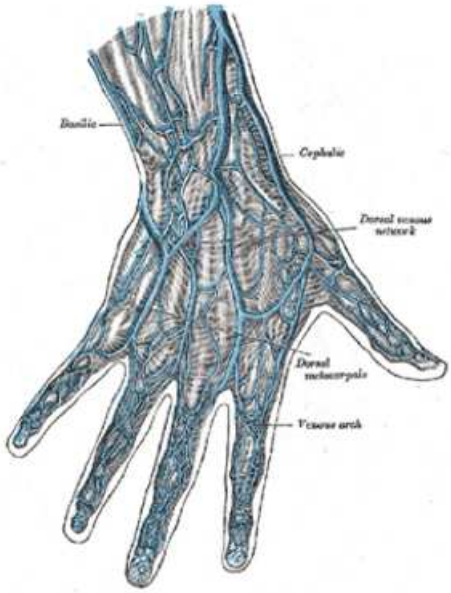

Figure 2.1. The veins on the dorsum of the hand [13]

2.2. Imaging for Vein Biometrics

When illuminated with a near-infrared light source, absorption of the veins is larger than other tissues. This causes veins to appear darker than other parts. Using this information, the veins that are closer to the skin surface are captured with the help of a near-infrared sensitive camera and an infrared light source.

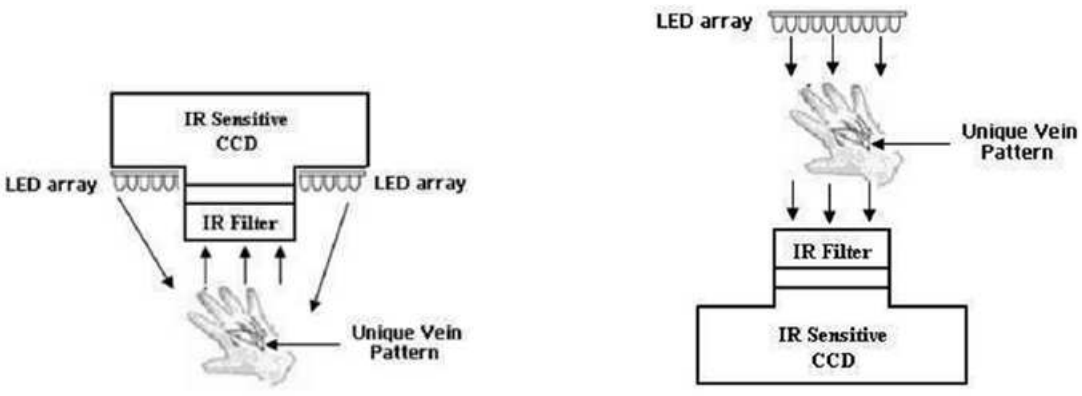

Figure 2.2. Configuration of a)Reflection based, b) Transmission based, acquision models [2]

The image of blood vessels can be acquired by either reflection or transmission methods as illustrated in Figure 2.2. In the reflection method, hand is placed in front of the camera and the light source, whereas in the transmission method the hand is placed between the camera and the light source. The reflection method is commonly preferred because the light transmittance is easily affected by temperature or weather. In the transmission method, if the hand's light transmission is high, the blood vessels are not visible in the image [2]. The configuration of vein capturing devices are different for each of the two method. In the reflection method, an illumination device and a capturing device can be combined because the direction of illumination and capturing is the same, but in the transmission method, those devices must be used separately because the direction of illumination and capturing differs.

Apart from the imaging methods, one has to decide which technique to use in order to capture the veins. There are two main imaging techniques: Far-Infrared (FIR) and Near-Infrared (NIR).

2.2.1. Near-Infrared (NIR) Imaging of Veins

In the entire electromagnetic spectrum, human eyes can only see the visible band, which is between $400 - 700\ nm$. Different objects reflect and emit light in different bands of the electomagnetic spectrum and there is useful information reflected by the objects of interest beyond the visible band. Although human vein patterns are not easily discernable in the visible band, they are easily captured in the near infrared band.

Biologically, there is a "medical spectral window" which extends approximately from 700 to 1000 nm, where light in this spectral window penetrates deeply into tissues, thus allowing for veins to be captured [14]. Therefore, the wavelength of the infrared light beam coming out from a light source should be within the near-infrared region. An exampe of this kind of imaging is given in Figure 2.3.

NIR imaging technique captures the major vein patterns in the back of the hand

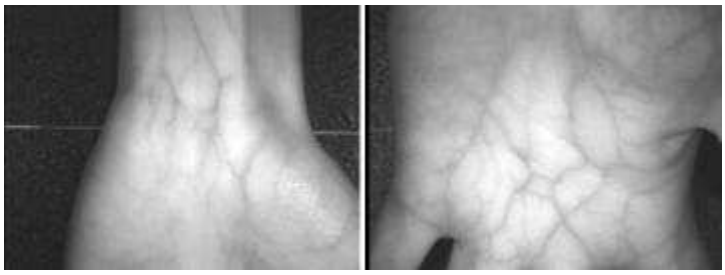

Figure 2.3. NIR images of the palm and wrist [5]

like FIR imaging technique. In addition, NIR imaging is capable of capturing images of the small veins lying in the palm and wrist areas. NIR imaging technique is more tolerant to the external environment and the subject's medical condition. However, when NIR imaging of vein patterns has defects on the skin surface that are also visible in the image, it will corrupt the structure of the vein patterns and lead to problems in later processing [5].

2.2.2. Far-Infrared (FIR) Imaging of Veins

It is known that when objects are heated, they emit infrared radiation. The Far-Infrared (FIR) imaging technology captures an image using the infrared radiation emitted by the human body. Having the knowledge that veins have higher temperature than the surrounding tissues, the images containing the heat distribution of body parts can be clearly captured by the thermal imaging in order to display the desired vein patterns. Different imaging technologies work within different spectral bands and FIR images are acquired in the spectral range of $8 - 14\ \mu m$. An example is given in Figure 2.4.

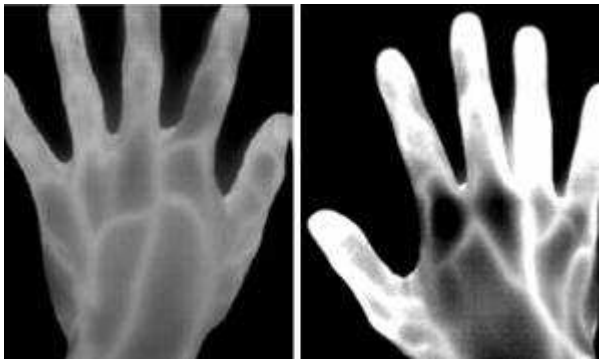

Figure 2.4. FIR images of the hand in an office environment [5]

FIR images have low levels of contrast that makes it difficult to separate the veins from the background. FIR imaging technology is very sensitive to external conditions. Also, the tissue near the blood vessels has similar temperature as the vein due to heat radiation under FIR imaging. In addition, as the FIR imaging can only capture the major vein patterns, the information contained in these patterns is limited and it is difficult to locate the exact position of a vein [5].

2.3. Hand Vein Database

We preferred to use NIR imaging technology in order to capture the vein patterns in the back of the hand. The hand vein image acquisition setup and the factors that affect the hand vein patterns are investigated in detail in this chapter.

2.3.1. Hand Vein Image Acquisition Setup

Since the hand vascular pattern lies under the skin, it can not be seen by the human eye. Therefore, we can not use visible light, which occupies a very narrow band ($300 - 500\ nm$ wavelength), for image acquisition. The principle is that the infrared light within the wavelength of $700 - 1000\ nm$ can pass through most of human tissues while the hemoglobin in the blood can absorb the infrared light fully [14] and causes the vascular patterns to appear as black patterns in resulting images. The absorption spectra of hemoglobin can be observed from Figure 2.5. Therefore, an infrared light source with proper wavelength is needed to shine the region of interest. Furthermore, a near-infrared sensitive camera has to be placed above the hand in order to capture the vein areas that become black under the infrared light source.

NIR imaging technology and reflection method is chosen for image acquisition part of this thesis. A monochrome NIR CCD camera WAT-902H2 ULTIMATE [15] attached with an infrared lens is used to capture the vein patterns in the back of the hand. This camera has a good sensitivity in the near infrared spectrum (Figure 2.6 [16]). The region of interest is irradiated by two IR light sources. Light sources are composed of 6 big infrared LEDs which are placed in a circular combination. Diffusing papers are

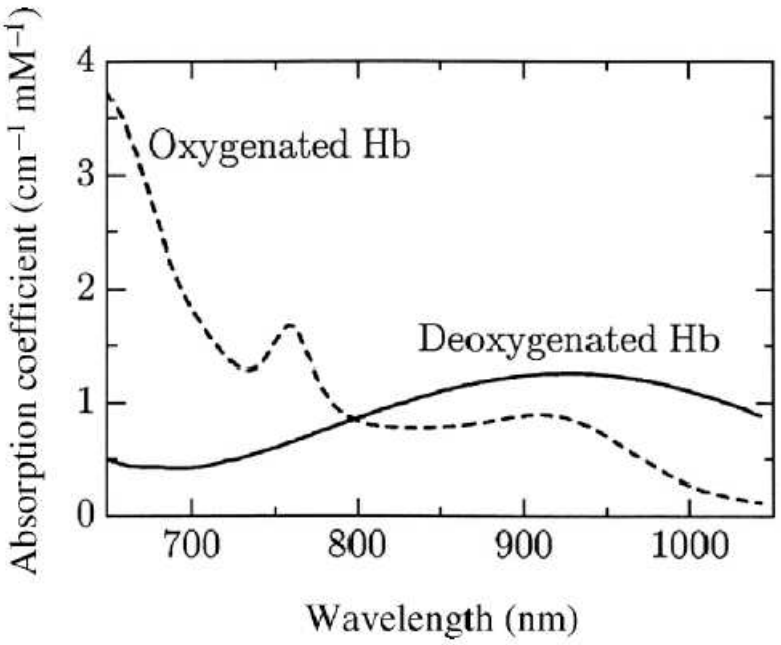

Figure 2.5. Absorption spectra of hemoglobin

placed in front of the infrared light sources to scatter the light uniformly. In order to eliminate the effects of visible light, the setup is installed in a dark room. The camera in the overhead position is adjusted approximately 80 cm above the hand stand. Users were asked to place their hands on a black sheet with the back of the hand facing the camera. The images were digitized into 640 × 480 pixels with a gray-scale resolution of 8-bit per pixel and after deinterlacing, the image sizes were reduced to 300 × 240 pixels.

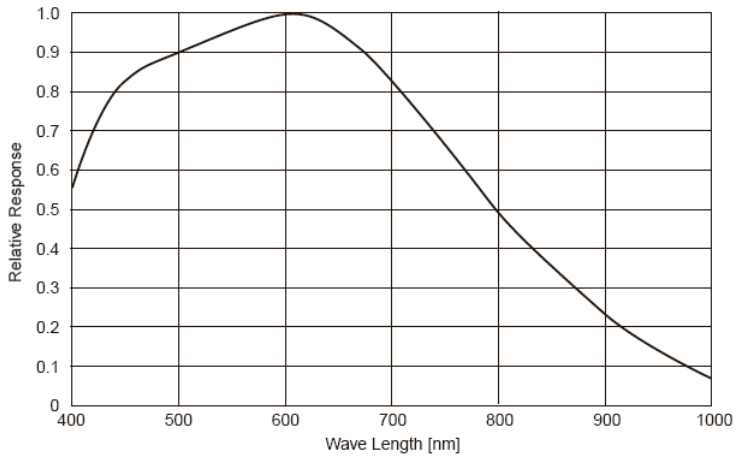

Figure 2.6. Acquisition camera's spectral response

2.3.2. Variability in Hand Veins

The database we constructed is acquired in different conditions taking into account the effects of temperature and physical activity. Furthermore, in order to see the effects of time lapse the images are captured again for a small subset of the database after approximately two months later from the first shot.

In Figure 2.7, the changes between different data collection conditions is presented for the same person. The veins become more visible after the stages of holding bag and ball squeezing since the blood flow to the region of interest is increased. On the other hand, after holding an ice pack, the veins become narrower and thus less visible. After having observed our hand vein images and the images that are reported in the

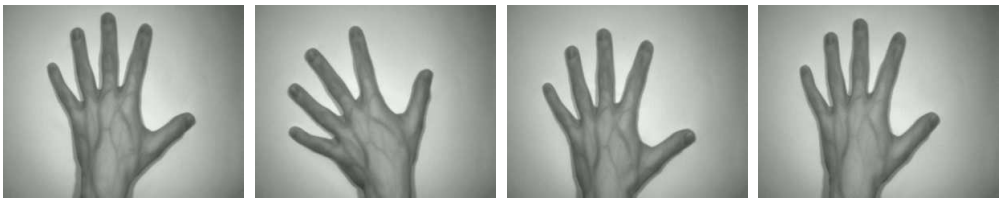

Figure 2.7. a) Image in normal condition b) After carrying a bag c) After doing the physical activiy d) After holding the ice.

literature, we can say that the quality of the hand vein images are affected by;

- Camera noise.
- Scattered light source.
- Position of the hand under the camera.
- Temperature.
- Hairs on the back of the hand.
- Depth of veins under the skin.
- Thickness of the veins.
- Amount of the subcutaneous fat.
- Darkness of the skin pigmentation.
- Birth marks, scars, etc.
- Age and gender.

- Physical activity.

Moreover, to understand the variability between hand vein images, capturing procedure is repeated hourly. When the hand vein images are observed in detail, the vein patterns do not change but in some cases they become less visible. This is due to the person's body temperature and the actions he/she performed. The images can be observed from Figure 2.8.

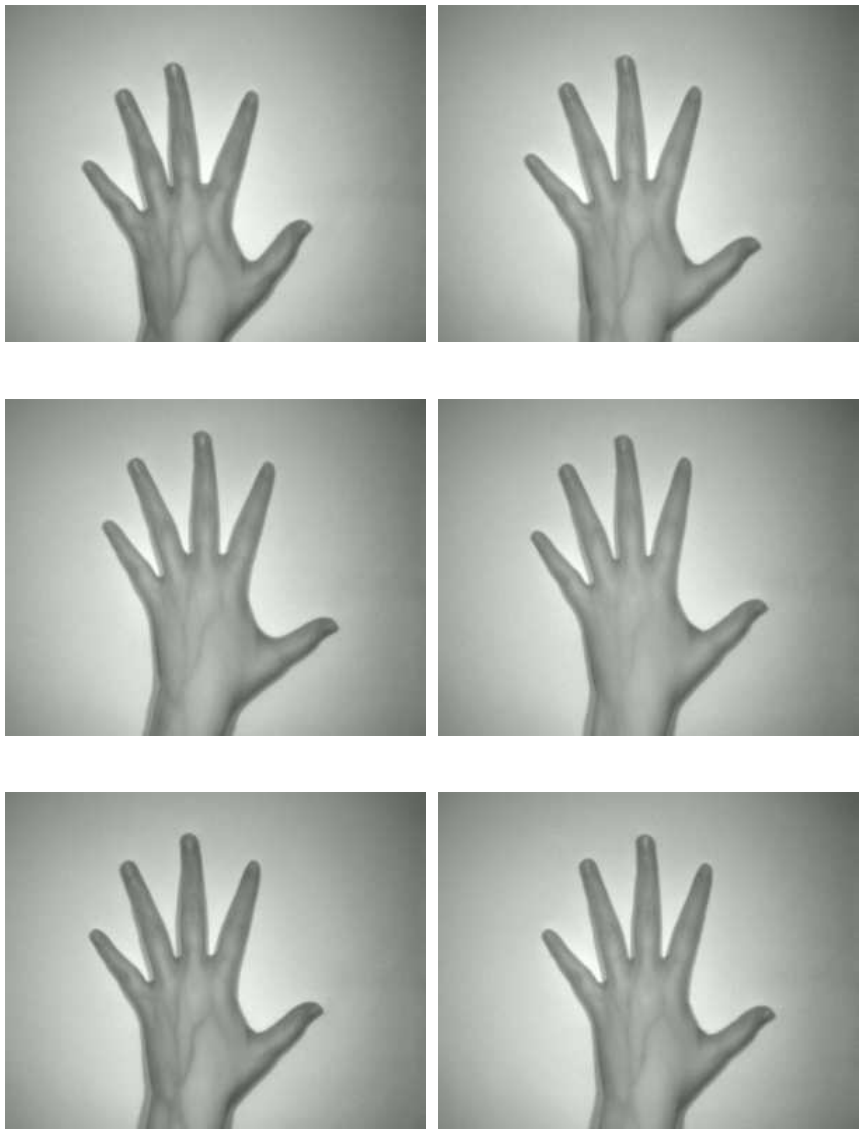

Figure 2.8. Hourly captured vein images

3. BIOMETRIC IDENTIFICATION FOR HAND VEINS

The hand vein identification system consists of six main steps of image acquisition, normalization of hand position, segmentation of the veins, feature exraction, identity matching and score/decision fusion. The details of the system can be observed from Figure 3.1.

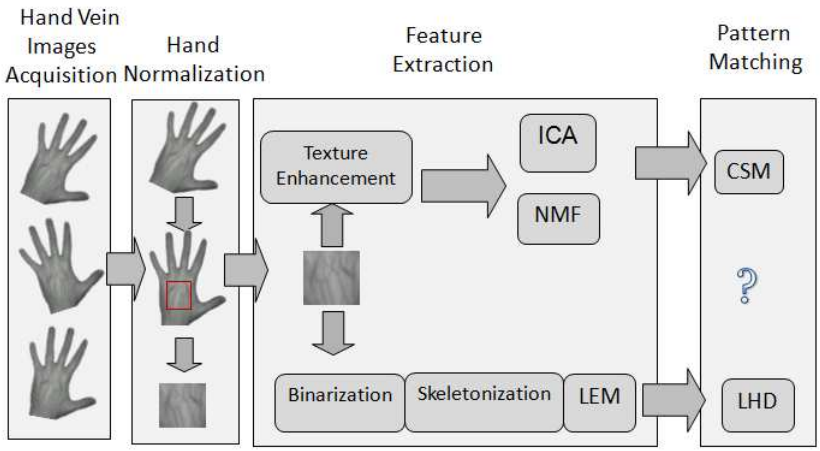

Figure 3.1. Identification steps for the hand vein biometry system

3.1. Image Acquisition

The data was collected from 100 people, 42 female and 58 male subjects. Three images were captured for each of the following conditions, hence overall twelve images per subject:

- Under normal condition,
- After having carried a bag weighing 3 kg. for one minute,
- After having squeezed an elastic ball repetitively (closing and opening) for one minute,
- After having cooled the hand by holding an ice pack on the surface of the back of the hand.

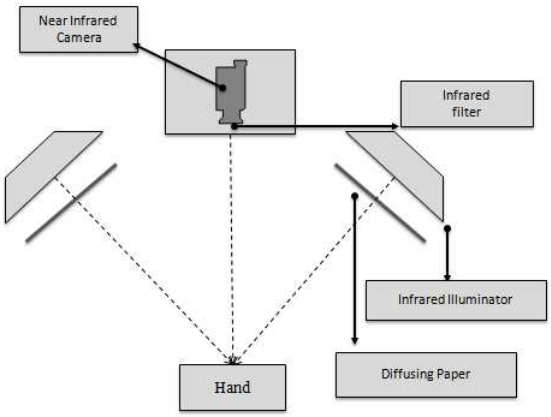

Figure 3.2. The hand vein image acquisition setup

First of all, users place their right hands and then left hands in front of the camera, and three images are taken in arbitrary poses. This session is named as "normal (N)"since no attempt to change vein pattern appearence is performed. Then, capturing proceeds with the left hand. Users are asked to carry a bag in their left hands, while standing up for one minute. Again three images are acquired and this process is named as "bag (B)". Then, the person is asked to squeeze an elastic ball, closing and opening the fist for one minute, namely "activity (A)". In the last session, an ice pack is placed on the back of hand and this session is named as "ice (I)". We observe that these actions, which simulate real life conditions have an effect on hand vein pattern appearence. In total, we obtain 1200 left hand images. In addition, 300 right hands in normal conditon are also acquired to determine the degree of interchangeability between the left and right hands. For each individual we are recording the following information with the vein images in our database:

- Acquisition date,
- Left/right handed information,
- Age,
- Gender,
- If the user doing any sport involving the hands?
- The user's job.

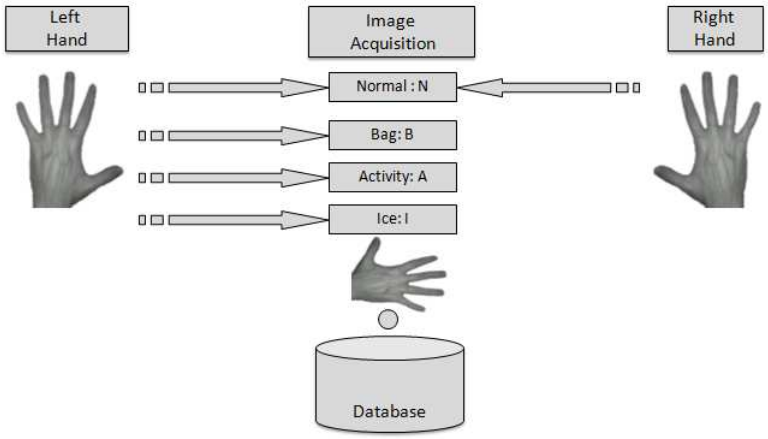

Figure 3.3. Data collection steps

The images are named as p(id)_(section name)_(image number).bmp. For example, for person 56, bag section and second image will be recorded as p56_bag_2.bmp. Other sections are named as 'bag' and 'act', and 'ice'.

Table 3.1. Database information

Gender	Female: 42 person, Male: 58 person
Left/Right Handed	Left: 2 person, Right: 98 person
Age	Varying between 16-63

3.2. Normalization of the Hand Position

In order to normalize the hand images and obtain the 100×100 vein region, we use Yoruk *et al.* algorithm [17, 18]. The normalization or registration task involves several consecutive processing steps, namely, segmentation of the hand image from the background, hand rotation and translation, finding the finger axes and tips, removal of ring artifacts, completion of the wrist, estimation of finger pivots, rotation and translation of fingers to standard orientations, Figure 3.5. Hand vein images and corresponding 100×100 vein images are shown in Figure 3.4

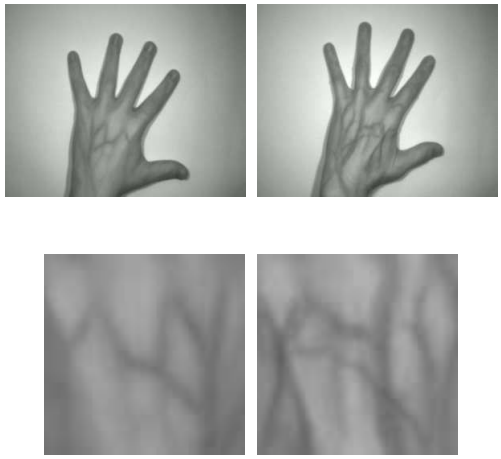

Figure 3.4. Hand vein images and region of interest images after normalization process

3.2.1. Hand Segmentation

Yoruk *et al.* algorithm starts with a two class K-means clustering algorithm to separate and extract the hand from the background is followed by morphological operators to fill in holes. The silhouette of the hand is extracted at the end of the segmentation stage.

3.2.2. Initial Hand Registration

The registration process of the algoritm involves translation of the centroid of the binary hand mass and its rotation in the direction of the larger eigenvector of the inertia matrix [19]. An ellipse fitted to the connected component of the hand object, where the larger eigenvalue determines the hand orientation and corresponds to themajor axis of the ellipse.

3.2.3. Finger Tips and Valleys

In order to detect and localize the hand extremities, that is, the fingertips and the valley between the fingers, the radial distances with respect to a reference point around the wrist region are computed. This reference point was taken as the first intersection

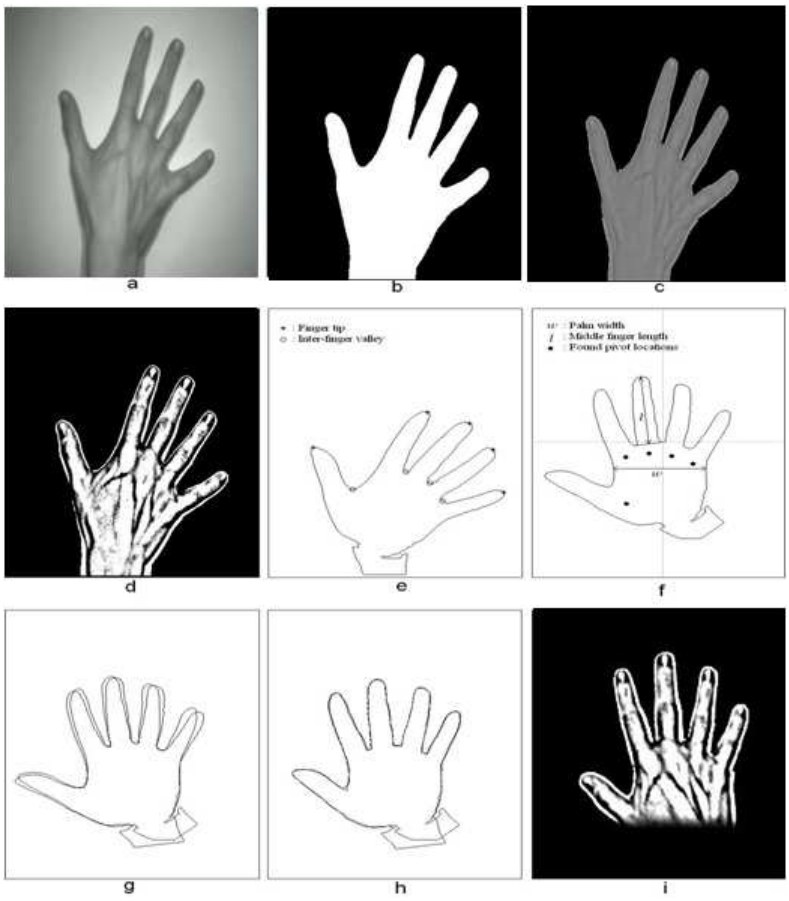

Figure 3.5. Processing steps for hand normalization: a) Original hand image; b) Segmented hand image; c) Illumination corrected hand image (ring removed); d) Gray-scale, texture enhanced hand image; e) Determination of finger tips and valleys; f) Initial global registration by translation and rotation: Middle finger length and palm width for hand image scaling and derivation of the metacarpal pivots; g) Superposed contours taken from different sessions of the same individual with rigid hand registration only; h) Superposed contours taken from different sessions of the same individual after finger orientation normalization; i) Final gray- scale, normalized hand with cosine-attenuated wrist [17, 18].

point of the major axis (the larger eigenvector of the inertial matrix) with the wrist line. The resulting sequence of radial distances yields 4 minima (finger valleys)and 5 maxima (finger tips) corresponding to the sought extremum points.

3.2.4. Wrist Completion

In order to create similar wrist contour for every hand image, wrist region is tapered off with a cosinusoidal window starting from the half distance between the pivot line and the wrist line. The wrist line is defined as the horizontal line passing through the estimated thumb pivot on the globally rotated hand image.

3.2.5. Finger Pivots

The fingers alignment process consists of reorientation of fingers along predetermined directions and around their metacarpal-phalanx pivots or finger pivots.

3.3. Vein Segmentation

Binarization is the quantization of the image into two levels; object (vein) and backgroud (non-vein). NIR produces images that need to be enhanced prior to further processing. Due to the fact that the gray level intensity values of the veins vary slowly across the image, global thresholding techniques do not provide satisfactory results.

3.3.1. Binarization Methods

We have applied four local binarization methods in order to segment the veins, namely, Yasuda [20], Bernsen [20], Niblack [20], Wang [5] and one global method, namely, Otsu [20].

3.3.1.1. Bernsen Method. In the local method of Bernsen [20], the threshold is set at the midrange value, which is the mean of the minimum $I_{low}(i, j)$ and maximum

$I_{high}(i,j)$ gray values in a local window, w=31. However, if the contrast $C(i,j) = I_{high}(i,j) - I_{low}(i,j)$ is below a certain threshold, then that neighborhood is said to consist only of one class, depending on the value of $T(i,j)$:

$$T(i,j) = \frac{1}{2}(local_{max} * I(i,j) - local_{min} * I(i,j)) \tag{3.1}$$

where $C(i,j) = I_{high} - I_{low} \geq 15$.

3.3.1.2. Niblack Method. The idea of this method is to vary the threshold over the image, based on the local mean and local standard deviation. The threshold at pixel (i,j) is calculated as:

$$T(i,j) = m(i,j) + k.\sigma_{i,j} \tag{3.2}$$

where $m(i,j)$ and $\sigma(i,j)$ are the sample mean and standard deviation values, respectively, in a local neighborhood of 15×15 and $k = -0.2$.

3.3.1.3. Wang Method. Due to the fact that the gray-level intensity values of the vein vary across the image, global thresholding techniques alone do not provide satisfactory results. Thus, the authors in [5] investigated an algorithm that combines global and local adaptive thresholding. Local thresholding with global reduction gives a more satisfactory result for segmenting the vein patterns from the background. The algorithm chooses different threshold values for every pixel in the image based on the analysis of its surrounding neighbors. For every pixel in the image, its threshold value is set as the regional mean value subtracted by a global offset.

$$I^{'}(x,y) = \begin{cases} 1, & I(i,j) \geq (\mu_{ij} - T_g) \\ 0, & \text{Otherwise.} \end{cases} \tag{3.3}$$

where μ_{ij} is the mean value for its 15×15 neighborhood, and $T_g = 2$ is a common offset for all the pixels.

3.3.1.4. Otsu Method. Otsu suggested minimizing the weighed sum of within-class variances of the foreground and background pixels to establish an optimum threshold. In Otsu's method we exhaustively search for the threshold that minimizes the within-class variance, defined as a weighed sum of variances of two classes:

$$\sigma_\omega^2(t) = \omega_1(t)\sigma_1^2(t) + \omega_2(t)\sigma_2^2(t) \tag{3.4}$$

weights w_i are the probabilities of the two classes seperated by a threshold t and σ_i^2 are variances of these classes. Otsu shows that minimizing the within-class variance is equivalent to maximizing the between-class variance:

$$\sigma_b^2(t) = \sigma^2 - \sigma_\omega^2(t) = \omega_1(t)\omega_2(t)(\mu_1(t) - \mu_2(t))^2 \tag{3.5}$$

3.3.1.5. Yasuda Method. In the Yasuda method [20] one first applies a normalization process, followed by a nonlinear smoothing, which preserves the sharp edges and culminating in an adaptive thresholding and segmentation stage. The smoothing consists of replacing each pixel by the average of its eight neighbors, provided the local pixel range is below a threshold T_1.

An adaptive threshold is applied, whereby any pixel value is attributed to the background (i.e., set to 255) if the local range is below a threshold T_2 or the pixel value is above the local average, both computed over $w \times w$ windows. Otherwise, the dynamic range is expanded accordingly. Finally, the image is binarized by declaring a pixel to be an object pixel if its minimum over a 3×3 window is below T_3 or its local variance is above T_4.

The algorithm has four steps;

(i) Normalization

$$f_1(x,y) = \frac{f(x,y) - \min}{\max - \min}$$

(ii) Smoothing

$$f_2(x,y) = \begin{cases} f_1(x,y), & \text{range}(x,y) > T_1; \\ \sum_{(x',y') \in A(x,y)} \dfrac{f_1(x',y')}{8}, & \text{Otherwise.} \end{cases}$$

(iii) Adaptive Threshold

$$f_3(x,y) = \begin{cases} 255, & \max b(i) < T_3 \text{ or } f_2(x,y) > ave\ b(i); \\ \dfrac{f_2(x,y) - \min b(i)}{ave b(i) - \min b(i)} 255, & \text{Otherwise.} \end{cases}$$

(iv) Segmentation

$$b(x,y) = \begin{cases} 1, & \min f_3(x,y) < T_3 \text{ or } \sigma(x,y) > T_4; \\ 0, & \text{Otherwise.} \end{cases}$$

3.3.2. Comparison of the Binarization Techniques

For comparison of these binarization techniques that are detailed in the previous section, the scores of various similarity criteria [20], such as accuracy, misclassification error (ME), Hausdorff distance and Modified Hausdorf (MHD) is presented. Based on several ground truth-images, these similarity criterias between ground-truth images and test images are calculated and summarized in Table 3.2. Based on the calculations the best results have been obtained with the Yasuda method.

3.3.2.1. Accuracy. Accuracy calculates the percentage of true classified vein pixels. It is defined as:

$$Accuracy = \frac{|B_O \cap B_T| + |F_O \cap F_T|}{|B_O| + |F_O|} \tag{3.6}$$

where B_O and F_O represent background and foreground of original (ground-truth) image, B_T and F_T denote the background and foreground area pixels in the test image.

3.3.2.2. Misclassification Error (ME). Misclassification Error (ME), reflects the percentage of background pixels wrongly assigned to foreground, and conversely, foreground pixels wrongly assigned to background. For the two-class segmentation problem, the definition is:

$$ME = 1 - \frac{|B_O \cap B_T| + |F_O \cap F_T|}{|B_O| + |F_O|} \tag{3.7}$$

where B_O and F_O represent background and foreground of original (ground-truth) image, B_T and F_T denote the background and foreground area pixels in the test image. The ME varies from 0 for a perfectly classified image and 1 for a totally wrong binarized image.

3.3.2.3. Hausdorff Distance (HD). The Hausdorff distance can be used to assess the shape similarity of the thresholded regions to the ground-truth shapes. Recall that, given two finite sets of points, say ground-truth and thresholded foreground regions, their Hausdorff distance is defined as:

$$H(F_O, F_T) = max\{d_H(F_O, F_T), d_H(F_T, F_O)\} \tag{3.8}$$

where, $d_H(F_O, F_T) = \max_{f_O \in F_O} d(f_O, F_T) = \max_{f_O \in F_O} \min_{f_T \in F_T} \|f_O, F_T\|$ and $\|f_O, F_T\|$ denotes the Euclidean distance of two pixels in the ground-truth and thresholded images.

3.3.2.4. Modified Hausdorff Distance (MHD). Since the original definition of the Hausdorff distance is rather sensitive to noise, a more robust version of this metric, namely the Modified Hausdorff Distance (MHD) is defined as;

$$MHD(F_O, F_T) = \frac{1}{|F_O|} \sum_{f_o \in F_O} d(f_O, F_T) \tag{3.9}$$

Table 3.2. Comparison of binarization methods

	Accuracy	ME	HD	MHD
Niblack	0.69	0.30	15.85	1.16
Bernsen	0.86	0.13	15.03	0.41
Yasuda	0.94	0.05	12.31	0.27
Wang	0.74	0.25	14.86	0.81
Otsu	0.78	0.21	29.65	2.04

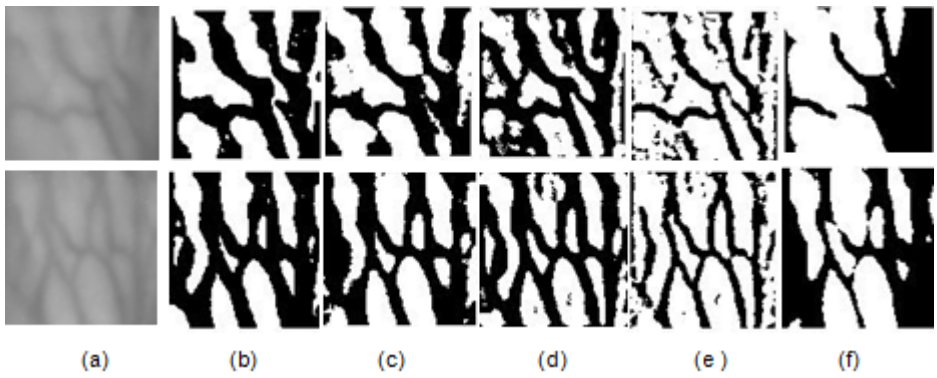

Figure 3.6. Output of different binarization methods on two vein images, (a) vein image (b) Yasuda (c) Bernsen (d) Wang (e) Niblack (f) Otsu

3.3.3. Skeletonization

After performing Yasuda binarization on the vein images, in order to eliminate the background noise, the area of the black and the white regions is calculated in a local window. If the area of the background is smaller than the given size, this block is

taken as noise and erased. Once a binary map is obtained, a skeletonization algorithm is applied to the connected components which yields the vein line segments.

The skeleton of a region is defined via the Medial Axis Transformation (MAT) [21]. In order to find the MAT of a region R with border b, for each point p in R, its closest neighbour in b is found. If p has more than one such neighbor, it is said to belong to the medial axis (skeleton) of R. For skeletonization bwmorph method with 'skel' option of Matlab is used.

3.4. Feature Extraction

In this thesis we have applied both apperance based and geometry based techniques. Appearance based methods such as Independent Component Analysis (ICA) or Non-negative matrix factorization (NMF) try to find a suitable representation of the original data while approximating the original data by keeping as much information as possible whereas geometry-based methods represent an object by its shape/contour. Appearance-based methods can be divided into two main classes, i.e., local and global approaches. Local feature is a property of an image located on a single point or small region. By contrast, global features try to cover the information of the whole image. The main idea of all of these methods is to project the original data onto a subspace, that represents the data optimally according to a predefined criterion: independency of the data (ICA), or non-negative, additive, components (NMF).

We have developed three hand recognition schemes applying both apperance based and geometry based methods. The first two recognition schemes consider the whole image and apply two different subspace methods, namely ICA and NMF. The third method, LEM is based on distances between the contours representing the hand veins, and hence it is shape-based.

3.4.1. Independent Component Analysis (ICA)

Independent Component Analysis (ICA) is a technique for extracting statistically independent variables from a mixture of them. It has been successfully used in many different applications for finding hidden factors within data to be analyzed or decomposing it into the original source signals. ICA assumes that each one of the observed signals $\{x_i(k), k = 1, .., K\}$, $i = 1, .., N$ is a mixture of a set of N unknown independent source signals s_i which are linearly combined through an unknown mixing matrix A. In ICA x_i and s_i are combined to form the X and S matrices. There are two architectures in the literature [22]. We apply both ICA architectures as a feature extraction tool on texture enhanced vein images. In ICA architecture I (ICA1), x_i and s_i are rows of $N \times K$ matrices and in ICA architecture 2 (ICA2), they are columns of $K \times N$ matrices. We have the following model:

$$X = AS \tag{3.10}$$

The data vectors for the ICA analysis are the lexicographically ordered hand image pixels. The dimension of these vectors is $K = 10000$, if we assume a 100×100 vein image. Briefly, ICA aims to find a linear transformation W for the inputs that minimizes the statistical dependence between the output components y_i, the latter being estimates of the hypothesized independent sources s_i:

$$S \cong WX \tag{3.11}$$

In order to find such a transformation W, which is also called separating or de-mixing matrix, we implemented the fastICA algorithm [23].

3.4.1.1. ICA Architecture I. In the first architecture, each of N individual hand-data vectors is assumed to be a linear mixture of an unknown set of N statistically independent source hands. For this model, images of normalized hands, of size 100×100 construct data vectors of size 10000. More explicitly, the data matrix X will be $N \times 10000$

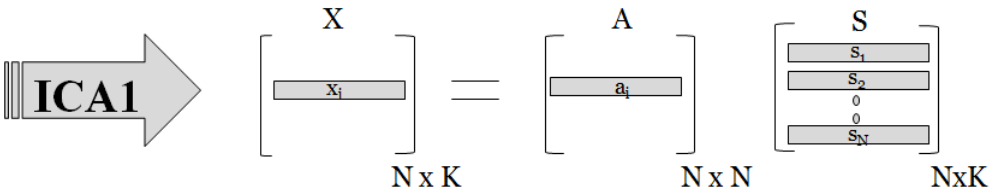

Figure 3.7. ICA architecture I

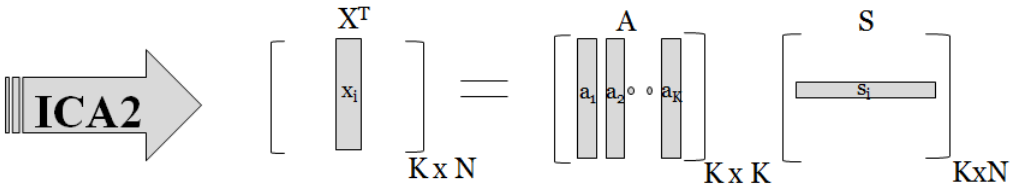

Figure 3.8. ICA architecture II

dimensional. This matrix is decomposed into N independent source components s_i, which will take place along the rows of the output matrix $S = WX$. Each row of the mixing matrix $A(N \times N)$, will contain weighting coefficients specific to a given hand. It follows then that, for the test hand x_i, the i^{th} row of A will constitute an N-dimensional feature vector. In our work, N was 100, since there were 100 subjects or "hand sources".

In the recognition stage, assuming that the test set follows the same synthesis model with the same independent components, we project a normalized test hand x_{test} (1×10000), onto the set of predetermined basis functions and compare the resulting vector of projection coefficients given by: $a_{test} = x_{test}S^T(SS^T)^{-1}$. Finally, the individual to be tested is simply recognized as the individual i when a_{test} is closest to the feature vector a_i.

3.4.1.2. ICA Architecture II. In the second architecture, the superposition coefficients are assumed to be independent, but not the basis images. Thus, this model assumes that, each of K pixels of the hand images result from independent mixtures of random variables. For this purpose, we start considering the transpose of the data matrix, X^T. We obtain our basis functions (the hand images) in the columns of the estimated

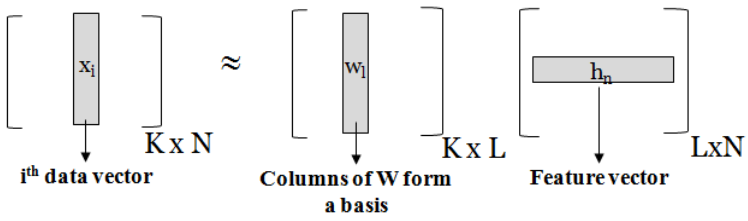

Figure 3.9. Non-negative Matrix Factorization

mixing matrix $A(N \times N)$. Conversely, the coefficients in the estimated source matrix are statistically independent. The number of pixels in the hand images was $K = 10000$, the number of subjects was $N = 100$, and finally the number of features used in the ICA2 architecture was $M = 100$.

3.4.2. Non-negative Matrix Factorization

Non-negative Matrix Factorization (NMF) is another matrix factorization technique with the added constraint that each factor matrix has only non-negative coefficients, i.e. all elements must be equal to or greater then zero [24]. Given a non-negative data matrix X of size $K \times N$, we obtain two non-negative matrices W and H such that:

$$X \cong WH \tag{3.12}$$

where W is of size $K \times L$ and H of size $L \times N$. Since we force the two matrices to be non-negative, we can only reconstruct X approximately from their product. The columns of W can be regarded as basis vectors and the columns of H are utilized as feature vectors of the corresponding vein images. We use Hoyer's code [25] for NMF representation.

3.4.3. Line Edge Map

Line Edge Map (LEM) is an approach that extracts lines from an image edge map as features. The algorithm can be considered as a combination of template matching and geometrical feature matching. It was proposed by Gao and Leung [26] and orig-

inally applied for face recognition. The steps of binarization, skeletonization and line extraction as adapted to vein images are detailed in the previous section. The basic unit of LEM is the line segment grouped from pixels of the edge map and matching of line segments is based on the Line Segment Hausdorff Distance (LHD). Two image patterns are considered to be similar if their LHD distance is small. LEM extraction

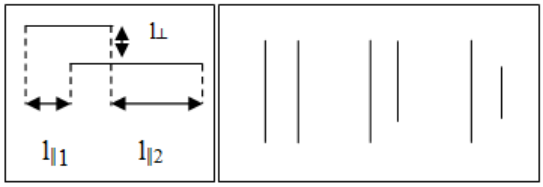

Figure 3.10. Perpendicular and parallel distances (right) and conditions (left) where $d_{\parallel}(m_i^l, t_j^l) = 0$ [26]

process mainly consists of four steps, binarization with Yasuda and noise removal, skeletonization of the binarized veins and line segments generation from these skeletons, Figure 3.11. The binarization and skeletonization of the images are discussed in Section 3.3 and Section 3.3.3 respectively.

In LEM generation process the vein patterns are divided into a number of line segments. From a given starting point, we track in one direction storing the coordinates of the edge points in an array and labeling the pixels in the edge image. We continue until no more connected points are found, or a junction point is encountered. At this point the function returns to the start point and tracks in the opposite direction (in its eight neighborhood). In the array of edge points, we find the size and position of the maximum deviation from the line that joins the endpoints, if the maximum deviation exceeds the allowable tolerance than the edge is shortened to the point of maximum deviation and the process is repeated. The start and end points of these lines are saved for LHD calculation.

3.4.3.1. Line Segment Hausdorff Distance. While Hausdorff Distance (HD) is a natural measure for comparing similarity of sets and shapes, its extension called Line Segment Hausdorff Distance (LHD) is a measure to compare line patterns. LHD incor-

porates structural information of line segment orientations and line-point associations, and hence is effective in comparing two shapes made up of a number of curve segments.

Figure 3.11. LEM extraction steps: Vein image, Yasuda binarization, noise removal, skeletonization and line segments generation

LHD measures the degree of dissimilarity between two LEMs. LEM is a representation which records only the end points of line segments on curves. An example LEM for the face matching problem is given in Figure 3.12. Given two LEMs, $M^l = \{m_1^l, m_2^l, .., m_p^l\}$ representing a model in the database and $T^l = \{t_1^l, t_2^l, .., t_q^l\}$ representing a test input LEM where the superscript l stands for line, LHD computes vectors such as $\vec{d}(m_i^l, t_j^l)$ that represents the dissimilarity between two line segments m_i^l and t_j^l. It is defined as:

$$\vec{d}(m_i^l, t_j^l) = \begin{bmatrix} d_\theta(m_i^l, t_j^l) \\ d_\parallel(m_i^l, t_j^l) \\ d_\perp(m_i^l, t_j^l) \end{bmatrix} \tag{3.13}$$

where $d_\theta(m_i^l, t_j^l)$, $d_\parallel(m_i^l, t_j^l)$ and $d_\perp(m_i^l, t_j^l)$ are the angular distance, parallel distance and perpendicular distance, respectively. The distance between the two line segments m_i^l and t_j^l is:

$$d\left(m_i^l, t_j^l\right) = \sqrt{\left(W_a d_\theta(m_i^l, t_j^l)\right)^2 + d_\parallel^2(m_i^l, t_j^l) + d_\perp^2(m_i^l, t_j^l)} \tag{3.14}$$

W_a, weight for angle distance, is taken as 20 emprically. Line Segment Hausdorff

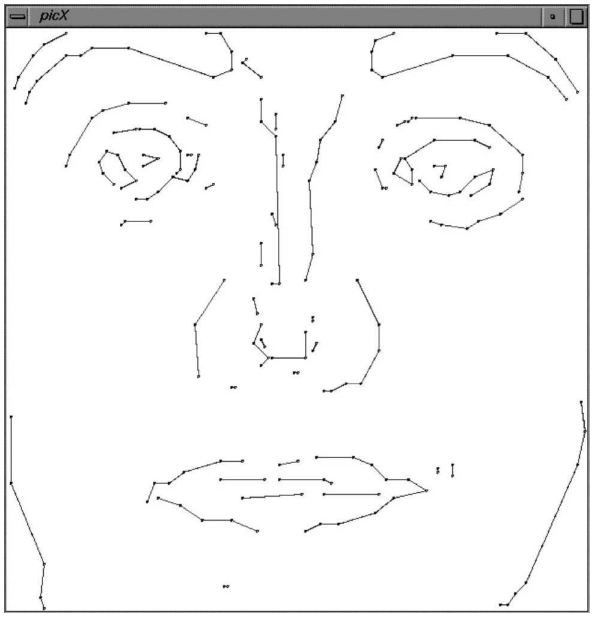

Figure 3.12. An illustration of a face LEM [26]

distance is defined as,

$$H_{LHD}\left(M^l, T^l\right) = \max\left(h\left(M^l, T^l\right), h\left(T^l, M^l\right)\right) \tag{3.15}$$

where,

$$h\left(M^l, T^l\right) = \frac{1}{\sum_{m_i^l \in M^l} l_{m_i^l}} \sum_{m_i^l \in M^l} l_{m_i^l} \cdot \min_{t_j^l \in T^l} d\left(m_i^l, t_j^l\right) \tag{3.16}$$

where, $l_{m_i^l}$ is the length of the line segment m_i^l.

$$d_\theta(m_i^l, t_j^l) = \tan\left(\theta\right) \tag{3.17}$$

$d_\theta(m_i^l, t_j^l)$, namely the angular distance computes the smallest intersection angle between lines m_i^l and t_j^l. Parallel and perpendicular distances are shown in Figure 3.10. Parallel distance can be calculated as,

$$d_\parallel(m_i^l, t_j^l) = \min\left(l_{\parallel 1}, l_{\parallel 2}\right) \tag{3.18}$$

LHD steps are given in Figure 3.14. These steps are:

(i) Two lines of different LEMs.
(ii) Calculate angular distance. $d_\theta(m_i^l, t_j^l) = \tan(\theta)$
(iii) Rotate shorter line to make them parallel.
(iv) Make them parallel to x axis, calculate perpendicular distance. $d_\parallel(m_i^l, t_j^l) = \min\left(l_{\parallel 1}, l_{\parallel 2}\right)$.
(v) Calculate parallel distance.

3.5. Identity Matching

Similarity scores for each algorithm are calculated using Cosine Similarity Metric (CSM) and Line Segment Hausdorff Distance (LHD) between test and template images. For ICA and NMF techniques, L1, L2 and CSM are calculated and the best results have been obtained with CSM. CSM is calculated as:

$$d_{cos}(a_i, a_{test}) = \frac{a_i \cdot a_{test}}{\|a_i\| \, \|a_{test}\|} \tag{3.19}$$

On the other hand, for LEM method, as described in Section 3.4.3.1, LHD is calculated between the line segments of the test LEM and enrollment LEM. LHD measures the degree of dissimilarity between two LEMs. Two image patterns are considered to be similar if their LHD distance is small.

3.6. Fusion Methods

We have considered four fusion techniques to improve the performance of the individual schemes used for the identification and verification tasks. We have used two score level fusion schemes and two decision level fusion schemes [27]. Combining different classifiers with the aim of increasing classification accuracy is a common technique in the pattern recognition discipline. Borda Count, Majority Voting, Z-score normal-

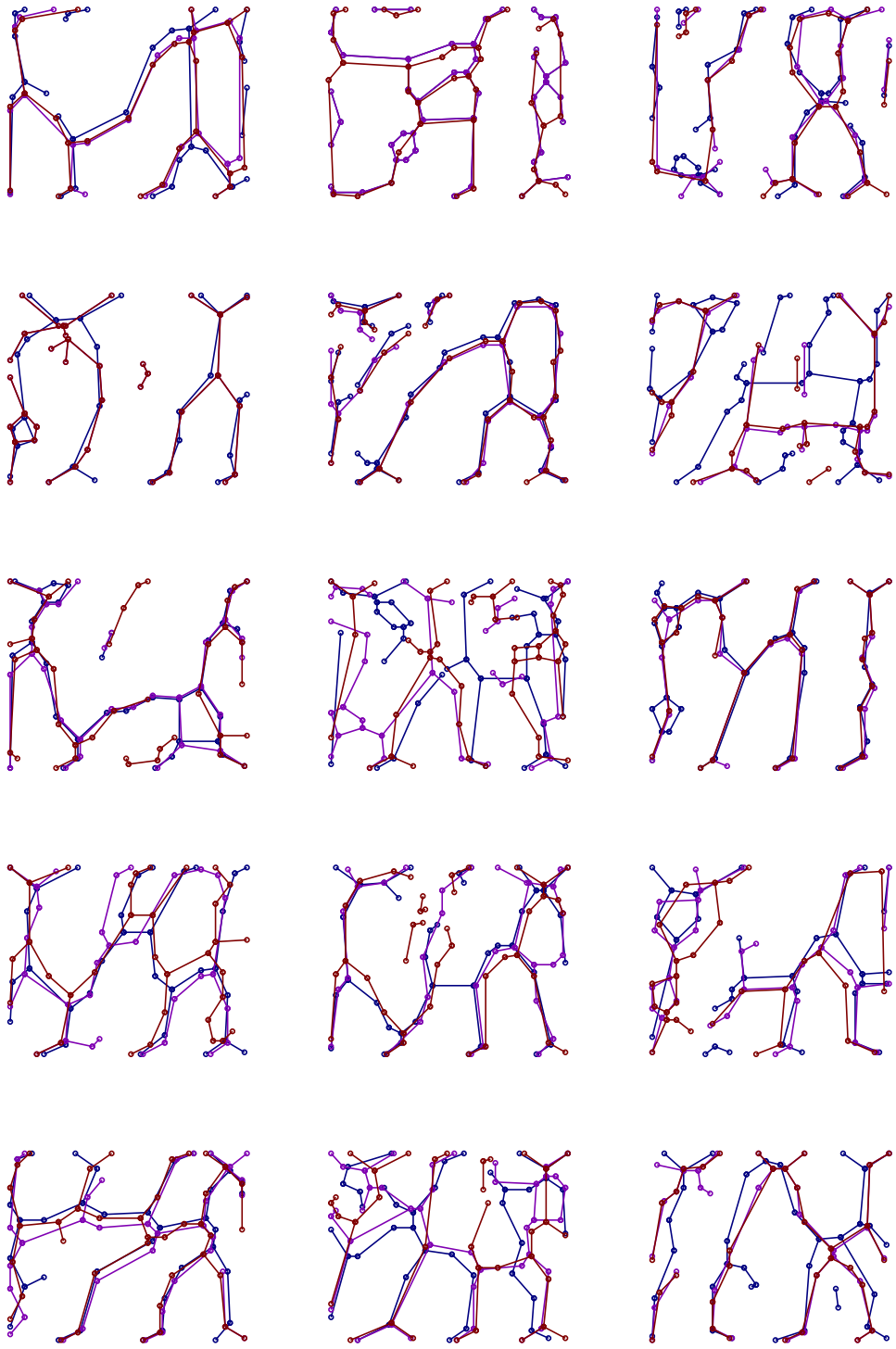

Figure 3.13. Three LEMs of the users are displayed on the same figure in order to see the variations

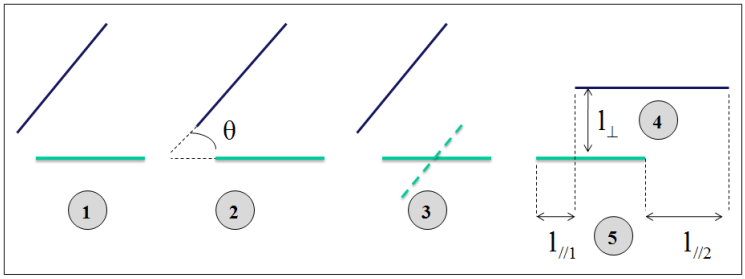

Figure 3.14. Calculation steps of parallel, angular and perpendicular distances

ized Sum and Product methods are used in order to fuse the results of the different classifiers.

3.6.1. Borda Count

Each method assigns its own rank to all the vein patterns in the database based on their distances to the input vein pattern. The ranks from individual schemes are summed up to obtain a final rank for each person in the database. Then the identity of the vein pattern is declared to be the one with the highest rank.

More explicitly, for a c class problem, ranks produced by any classifier C_i are in the range of $[1, .., c]$, where 1 is the topmost rank that denotes the highly probable class. Assume that classifier C_i outputs binary valued vectors $\{d_{i,1}, ..., d_{i,c}\}^T$, where $d_{i,j} \in 1, .., c$ then Borda count method simply selects the class label which has the minimum total rank:

$$arg \min_{j=1}^{c} \sum_{i=1}^{L} d_{i,j} \tag{3.20}$$

3.6.2. Majority Voting

Majority voting can be defined as follows: Assume that classifier C_i outputs binary valued vectors $\{d_{i,1}, ..., d_{i,c}\}^T \in [0, 1]$, $i = 1, .., L$, where L is the number of classifiers, and c is the number of the classes. $d_{i,j} = 1$ if classifier C_i thinks that the

unknown pattern belongs to ω_i, and $d_{i,j} = 0$ otherwise, i.e. each method assigns 1 if the classifier decides that the unknown pattern belongs to the class and assigns 0 otherwise. The class having the highest vote is declared to be the unknown pattern x's class.

$$arg \max_{j=1}^{c} \sum_{i=1}^{L} d_{i,j} \tag{3.21}$$

3.6.3. Fixed Arithmetic Combination Rules

When the individual classifiers produce class similarity scores, these scores can be combined by using simple arithmetic rules such as sum, product,min and max rules. Assume that classifier C_i outputs continuous valued score values $\{d_{i,1}, ..., d_{i,c}\}^T$, where $d_{i,j} \in [0, .., 1]$. Without any loss of generality, assume that greater values close to 1 mean high similarity. The following equations are used in order to make a decision:

- Sum Rule:

$$arg \max_{j=1}^{c} \sum_{i=1}^{L} d_{i,j} \tag{3.22}$$

- Product Rule:

$$arg \max_{j=1}^{c} \prod_{i=1}^{L} d_{i,j} \tag{3.23}$$

- Max Rule:

$$arg \max_{j=1}^{c} (\max_{i=1}^{L} [d_i, j]) \tag{3.24}$$

Note that arithmetic rules assume the classifier outputs to be in a common range. It is therefore necessary to normalize scores before fusing them. There are several ways to perform score normalization:

(i) Min-max Normalization If the bounds of the score values are known, or can be estimated, min-max normalization can be easily applied to normalize scores. Let d be the original score value. The normalized score can be computed as:

$$d^{'} = \frac{d - d_{MIN}}{d_{MAX} - d_{MIN}} \tag{3.25}$$

where d_{MAX} and d_{MIN} represent the minimum and maximum values of the score range. Depending on the application, d_{MAX} and d_{MIN} values may be known beforehand. Otherwise, they are generally estimated from the training set.

(ii) Z-score Normalization z-score normalization method transforms the raw scores into a new range with the help of sample arithmetic mean and standard deviation as follows:

$$d^{'} = \frac{d - \mu}{\sigma} \tag{3.26}$$

where μ and σ denote sample arithmetic mean and standard deviation, respectively.

4. EXPERIMENTAL RESULTS

We experimented with the techniques described in Chapter 3 using the hand vein database we collected, as described in Chapter 2. The hand vein database we used contains 1200 images of left hands of 100 different people, each person having three images of his left hand under four different conditions. The images have been collected in arbitrary poses and there were no control pegs to orient the fingers.

4.1. Methodology

For each individual, three hand vein images were recorded, denoted by the sets 1, 2, 3 and four different session are N, B, A, I, denoting images collected under normal condition, after bag carrying exercise, after ball pressing exercise and after having cooled with ice.

4.1.1. Identification Versus Verification

Associating an identity with an individual is called personal identification. The problem of resolving the identity of a person can be categorized into two types of problems: verification and identification. Verification or authentication refers to the problem of confirming or denying a person's claimed identity and identification refers to the problem of establishing a person's identity without any such claim.

In identification mode (one-to-many matching), the user does not provide any identity claim, but the system must find out the user's identity from a database of enrolled users. For the person identification task, we measure the similarity scores between the test feature vector and all the feature vectors in the database belonging to N different subjects and confirm the identified user as the person whose hand vein feature data has the maximum similarity score.

For a person verification task, one must differentiate the genuine hand from the

impostor hands as the user provides her hand image in support of her claimed identity. For this purpose, the distances between the hand of the applicant and all the hands in the database are calculated and the scores are compared against a threshold.

Feature organization and classification methods are identical for the LEM method and the subspace (ICA, NMF) methods, except that subspace methods use Cosine Similaritiy Metric (CSM) while LEM uses Line Segment Hausdorff Distance (LHD).

4.1.2. Different Enrollment Set Sizes

In order to see the effect of enrollment size, we ran the identification experiments with different enrollment sets. As enrollment sets, we used only "normal"images and as well as all images. In the single enrollment experiments that we use normal images as enrollment sets, the ordering of the enrollment sets were {(N1), (N2), (N3)} and the test sets were {(N2,N3), (N1,N3), (N1,N2), (B1,B2,B3), (A1,A2,A3), (I1,I2,I3)}. For instance, in one experiment, the enrollment set was N1 (100 left hands under normal conditions), and the test set was (N2,N3), the 200 hand images under normal condition while it was the 300 hands images (A1,A2,A3) after ball pressing exercise. In double enrollment experiments, the enrollment sets were {(N1,N2), (N2,N3), (N3,N1)} and the test sets were {(N3), (N1), (N2), (B1,B2,B3), (A1,A2,A3), (I1,I2,I3)}. More explicitly, for single enrollment tests, that we used normal images for enrollment (TEST1),

- Enrollment: {(N1)} and Test: {(N2,N3),(B1,B2,B3),(A1,A2,A3) and (I1,I2,I3)}
- Enrollment: {(N2)} and Test: {(N1,N3),(B1,B2,B3),(A1,A2,A3) and (I1,I2,I3)}
- Enrollment: {(N3)} and Test: {(N1,N2),(B1,B2,B3),(A1,A2;A3) and (I1,I2,I3)}

For double enrollment tests, that we used normal images for enrollment (TEST2),

- Enrollment: {(N1,N2)} and Test: {(N3),(B1,B2,B3),(A1,A2,A3) and (I1,I2,I3)}
- Enrollment: {(N2,N3)} and Test: {(N1),(B1,B3,B3),(A1,A2,A3) and (I1,I2,I3)}
- Enrollment: {(N1,N3)} and Test: {(N2),(B1,B2,B3),(A1,A2,A3) and (I1,I2,I3)}

For 4× enrollment tests that we used all images for enrollment (TEST3),

- Enrollment: {(N1,B1,A1,I1)} and Test: {(N2,N3),(B2,B3),(A2,A3) and (I2,I3)}
- Enrollment: {(N2,B2,A2,I2)} and Test: {(N1,N3),(B1,B3),(A1,A3) and (I1,I3)}
- Enrollment: {(N3,B3,A3,I3)} and Test: {(N1,N2),(B1,B2),(A1,A2) and (I1,I2)}

For 8× enrollment tests that we used all images for enrollment (TEST4),

- Enrollment: {(N1,N2),(B1,B2),(A1,A2) and (I1,I2)} and Test: {(N3,B3,A3,I3)}
- Enrollment: {(N2,N3),(B2,B3),(A2,A3) and (I2,I3)} and Test: {(N1,B1,A1,I1)}
- Enrollment: {(N1,N3),(B1,B3),(A1,A3) and (I1,I3)} and Test: {(N2,B2,A2,I2)}

4.1.3. Time Lapse

In order to see the effect of time lapse on the applied algorithms results, database collection process is repeated after three months. For 25 people from the database, the left hand images under normal condition have been collected. The former collected set is named as "Version 1"and the latter collected images are named as "Version 2"and the performance comparisons are provided for each set.

4.2. Performance Measures

For identification experiments, identification rates and for verification experiments, Equal Error Rates (EER) and Receiver Operating Characteristics (ROC) curves have been provided.

4.2.1. Identification Rate

Identification Rate is calculated by dividing the number of true classified tests to the number of all tests.

4.2.2. Equal Error Rate

Equal Error Rate (EER) is the rate at which both false accept and false reject rates are equal. The value of the EER can be easily obtained from the ROC curve. The EER is an effective way to compare the performances of different systems with different ROC curves. In general, the lower the EER the more accurate the system is considered to be. It can be easily read from the ROC plot by taking the point where FAR and FRR have the same value.

4.2.3. Reciever Operating Characteristics Curve

The Reciever Operating Characteristic Curve (ROC) plot is a visual characterization of the trade-off between the False Accept Rate (FAR) and the False Reject Rate (FRR). In general, the matching algorithm performs a decision based on a threshold which determines how close a template to the input needs to be in order to be considered a match. More implicitly, ROC curve plots, parametrically as a function of the decision threshold, the rate of "false positives"(i.e. impostor attempts accepted) on the x-axis, against the corresponding rate of "true positives"(i.e. genuine attempts accepted) on the y-axis. ROC curves are threshold independent, allowing performance comparison of different systems under similar conditions, or of a single system under differing conditions [28]. If the threshold is reduced, there will be less false non-matches but more false accepts. Correspondingly, a higher threshold will reduce the FAR but increase the FRR.

4.3. Experiments

The results for the single, double, 4× and 8× enrollment tests and the fusion results for each test have been provided in this section. For the identification experiments we provide identification rate and for verification experiments, we provide Equal Error Rate (EER) and Receiver Operating Characteristics (ROC) curve for the same test and enrollment sets.

Table 4.1. Results for single enrollment (TEST1): Identification rates and equal error rates (EER) for verification

Test Set		ICA1	ICA2	NMF	LEM
N1N2N3	Iden.Rate:	88.66	**94.16**	81.33	68.5
	EER:	4.02	**2.47**	8.14	13.52
B1B2B3	Iden.Rate:	**78.33**	72.33	71.44	73.77
	EER:	**8.01**	13.04	12.77	12.13
A1A2A3	Iden.Rate:	**75.55**	68.88	68.88	71.77
	EER:	**9.20**	13.23	14.11	12.76
I1I2I3	Iden.Rate:	**68.77**	64.88	66.55	65.77
	EER:	**11.52**	14.88	15.08	14.07
All	Iden.Rate:	**77.82**	75.06	72.06	69.95
	EER:	**8.18**	10.90	12.53	13.12

Table 4.2. Fusion results of ICA1, LEM and NMF for single enrollment (TEST1)

Test Set	ICA1	Majority Voting	Borda Count	Sum	Product
N1N2N3	88.66	86.33	86.00	**86.66**	85.66
B1B2B3	78.33	77.33	79.00	**80.77**	79.87
A1A2A3	75.55	75.00	76.22	78.66	**78.77**
I1I2I3	68.77	72.44	73.44	**74.88**	74.33
All	77.82	77.78	78.67	**80.25**	79.67

4.3.1. TEST1: Results for Single Enrollment

Results of the single enrollment experiments are given in Table 4.1. We have considered two score-level fusion schemes and two decision-level fusion schemes with the hope to improve the performance of the individual schemes used for the identification and verification tasks that are detaily explanied in Section 3.6. In Table 4.1, the best performances have been displayed in boldface. It is observed that for normal test set, ICA2 performs the best while for the other test sets involving stressed conditions, ICA1 performs superiorly.

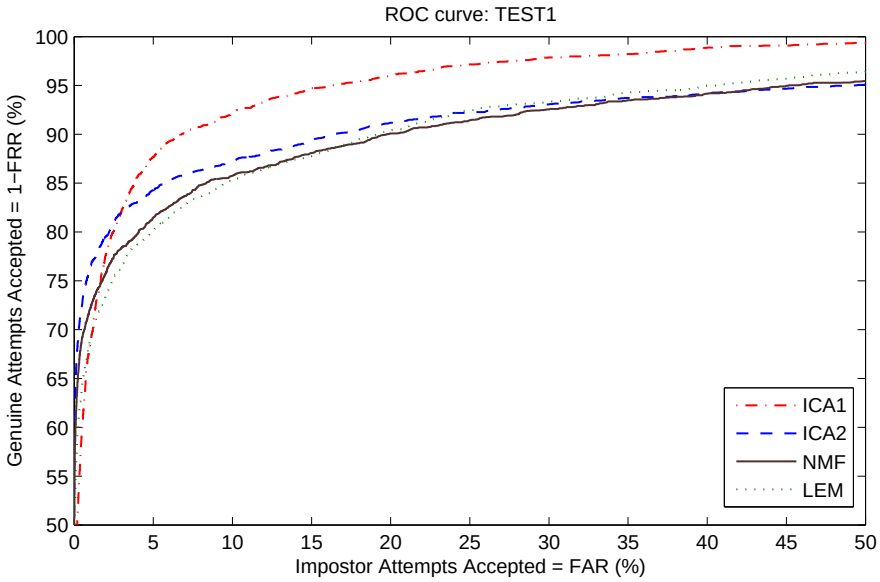

Figure 4.1. ROC curves: Single enrollment (TEST1)

4.3.2. TEST 2: Results for Double Enrollment

The identification rates increases and EER decreases when one moves from single enrollment to double enrollment, i.e. better performances have been obtained for double enrollment (TEST2). Results of the double enrollment experiments are given in Table 4.3 and the best performances have been displayed in boldface. It is observed that for normal test set, ICA2 performs the best while for the other test sets involving stressed conditions, ICA1 performs superiorly.

Score fusion under the Sum rule seems to perform slightly better than fusion under the Majority Voting, Borda Count and Product rules. Fusion of {ICA1,ICA2,NMF,LEM}, {ICA1,NMF,LEM} and {ICA2,NMF,LEM} have been performed but the best results have been obtained with the fusion of {ICA1, NMF, LEM}, thus results of this fusion have been provided. According to the results, fusing of the three methods {ICA1, NMF,LEM} outperforms the individual techniques.

For both single and double enrollment tests, ICA1 outperformed ICA2, NMF and LEM. Thus, we have given the ICA1 results on the same ROC curve in Figure 4.4.

Table 4.3. Results for double enrollment (TEST2): Identification rates and equal error rates (EER) for verification

Test Set		ICA1	ICA2	NMF	LEM
N1N2N3	Iden.Rate:	94.33	**97.33**	89.67	81.66
	EER:	2.43	**1.53**	4.00	7.41
B1B2B3	Iden.Rate:	**88.55**	82.88	83.33	88.44
	EER:	**4.75**	8.69	7.33	7.33
A1A2A3	Iden.Rate:	**86.44**	79.44	81.89	**86.66**
	EER:	**6.22**	8.00	8.33	6.47
I1I2I3	Iden.Rate:	77.66	74.77	77.22	**80.77**
	EER:	**8.22**	10.76	10.89	9.13
All	Iden.Rate:	**86.74**	83.60	83.03	84.38
	EER:	**5.40**	7.24	7.64	7.59

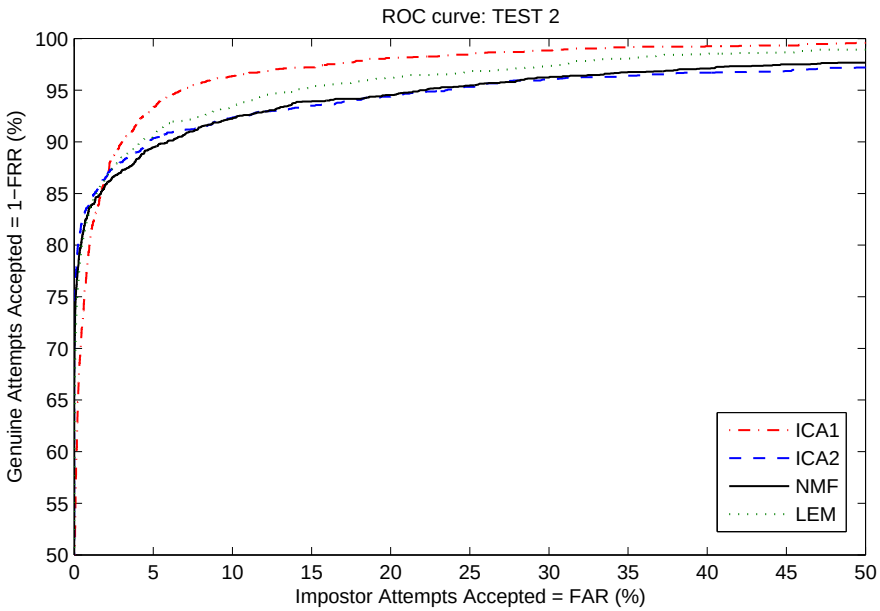

Figure 4.2. ROC curves: Double enrollment (TEST2)

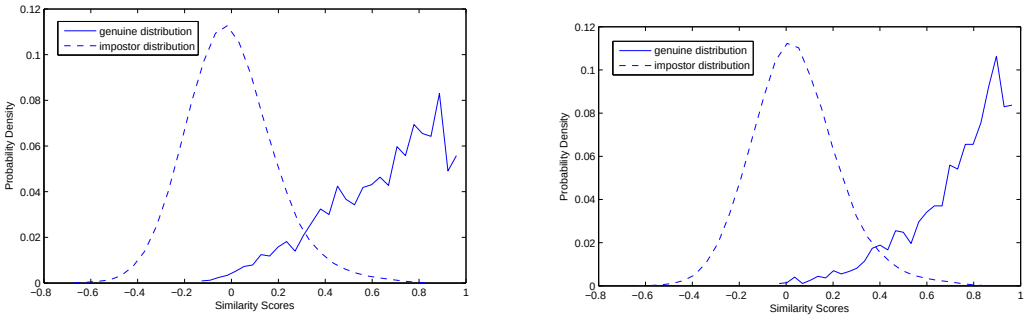

Figure 4.3. Genuine-impostor distributions, ICA1: TEST1 and TEST2

Table 4.4. Fusion results of ICA1, LEM and NMF for double enrollment (TEST2)

Test Set	ICA1	Majority Voting	Borda Count	Sum	Product
N1N2N3	94.33	93.00	93.00	**93.66**	92.00
B1B2B3	88.55	88.44	89.88	**91.33**	91.11
A1A2A3	86.44	87.33	87.55	**89.22**	**89.22**
I1I2I3	77.66	82.88	84.77	**85.44**	85.00
All	86.74	87.91	88.80	**89.91**	89.33

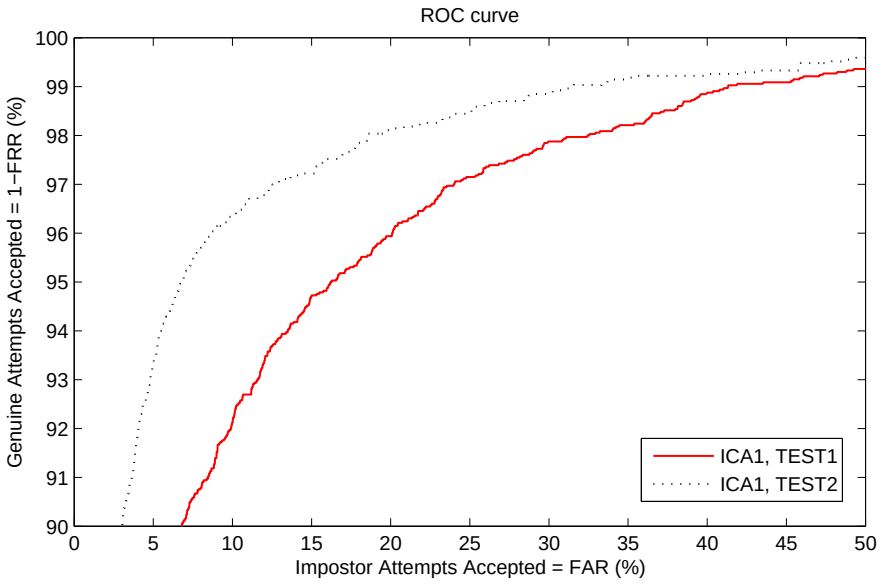

Figure 4.4. ICA1, ROC curve: Single (TEST1) and double enrollment (TEST2)

Table 4.5. Results for 4× enrollment (TEST3): Identification rates and equal error rates (EER) for verification

Test Set		ICA1	ICA2	NMF	LEM
N1N2N3	Iden.Rate:	94.33	**95.33**	92.83	87.66
	EER:	3.71	**1.83**	4.49	5.86
B1B2B3	Iden.Rate:	**91.83**	89.33	90.50	92.00
	EER:	**4.86**	5.79	5.21	**4.18**
A1A2A3	Iden.Rate:	**91.00**	89.16	89.66	92.00
	EER:	**4.98**	5.03	5.50	**4.63**
I1I2I3	Iden.Rate:	**89.50**	87.33	89.50	89.16
	EER:	5.83	4.95	**4.48**	5.51
All	Iden.Rate:	**91.67**	90.29	90.63	90.21
	EER:	**4.85**	**4.41**	4.92	5.05

Table 4.6. Fusion results of ICA1, LEM and NMF for 4× enrollment (TEST3)

Test Set	ICA1	Majority Voting	Borda Count	Sum	Product
N1N2N3	94.33	93.83	94.16	**95.16**	95.16
B1B2B3	91.83	92.50	94.00	**94.66**	94.66
A1A2A3	91.00	92.16	93.50	**95.16**	95.00
I1I2I3	89.50	92.50	93.00	**95.00**	94.50
All	91.67	92.75	93.67	**95.00**	94.83

4.3.3. TEST3: Results for 4× Enrollment

In the former tests of TEST1 and TEST2, we have used only normal images for enrollment. In the tests of TEST3 and TEST4 we used all images, i.e normal, bag, activity and ice images, as enrollment sets. The detailed information about the enrollment and test sets can be observed from Section 4.1.2. In Table 4.5, the best performances have been displayed in boldface. It is observed that for normal test set, ICA2 performs the best while for the other test sets involving stressed conditions, ICA1 performs superiorly.

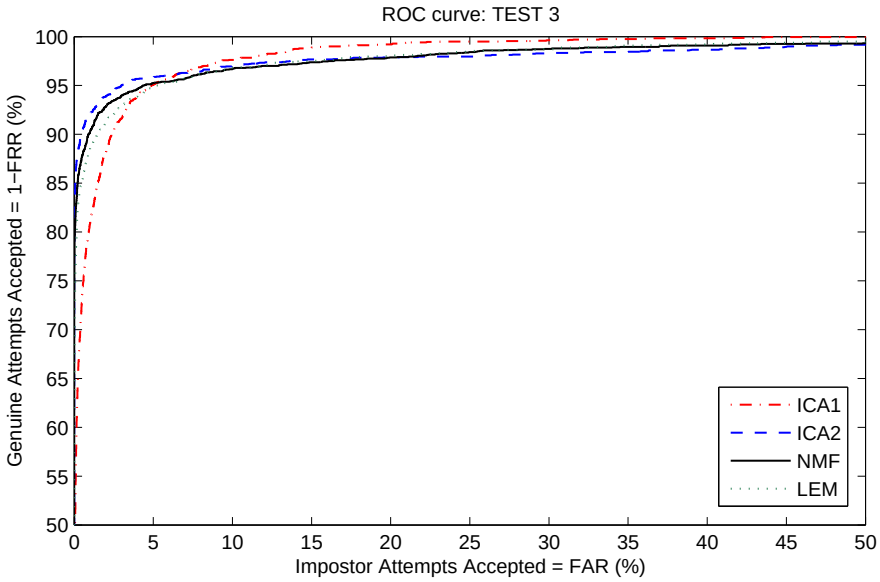

Figure 4.5. ROC curves: 4× enrollment (TEST3)

4.3.4. TEST4: Results for 8× Enrollment

In Table 4.7, it is observed that for normal test set ICA2, for bag test set LEM, for activity test set ICA1 and LEM and for ice test set NMF performs the best. Table 4.5 and Table 4.7 indicate that there is significant improvement when one shifts from single enrollment set to larger enrollment sets.

4.3.5. Resolution and Population Size Tests

In order to see the effect of the image resolution on the performance of the system, we have used different images of different resolutions: 30×30, 50×50, 70×70 and 100×100. Calculating EER on ICA1 algorithm, the results revealed that when the resolution decreases, the performance of the system also decreases, Figure 4.7. In Figure 4.8, the EER for different sized populations can be observed. As the population size increases, the performance decreases slightly.

Table 4.7. Results for 8× enrollment (TEST4): Identification rates and equal error rates (EER) for verification

Test Set		ICA1	ICA2	NMF	LEM
N1N2N3	Iden.Rate:	97.00	**98.66**	96.33	94.33
	EER:	2.29	**1.02**	2.00	3.44
B1B2B3	Iden.Rate:	97.00	94.66	95.00	**98.00**
	EER:	3.31	3.00	3.02	**1.74**
A1A2A3	Iden.Rate:	**98.00**	96.00	96.00	**98.00**
	EER:	**2.94**	2.33	2.37	**2.60**
I1I2I3	Iden.Rate:	94.66	94.33	**95.66**	94.66
	EER:	4.13	2.64	**2.00**	3.39
All	Iden.Rate:	**96.67**	95.92	95.75	96.25
	EER:	3.17	**2.25**	2.35	2.79

Table 4.8. Fusion results of ICA1, LEM and NMF for 8× enrollment (TEST4)

Test Set	ICA1	Majority Voting	Borda Count	Sum	Product
N1N2N3	97.00	97.66	98.00	**98.33**	98.33
B1B2B3	97.00	95.66	95.00	**97.33**	97.00
A1A2A3	98.00	76.44	98.33	**98.33**	98.33
I1I2I3	94.66	96.33	98.00	**98.66**	98.33
All	96.67	91.52	97.33	**98.16**	98.00

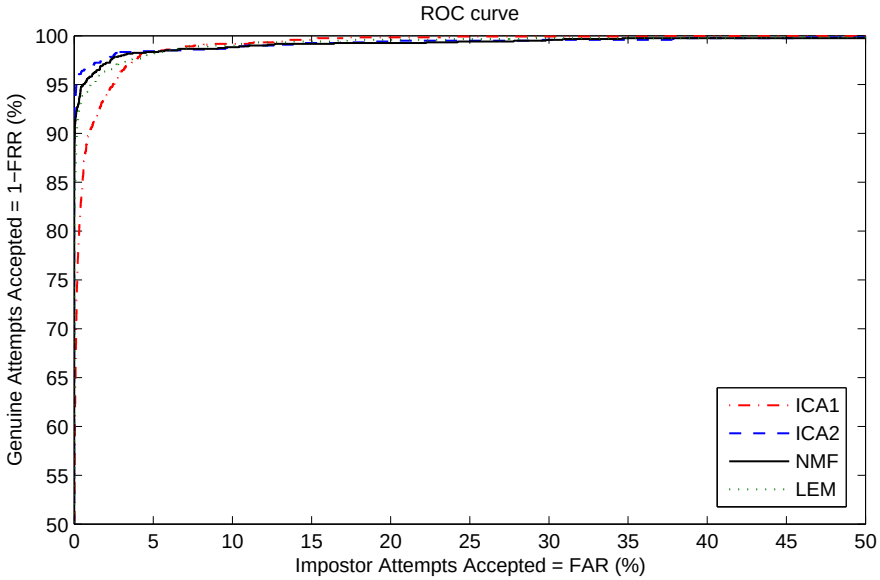

Figure 4.6. ROC curves: 8× Enrollment (TEST4)

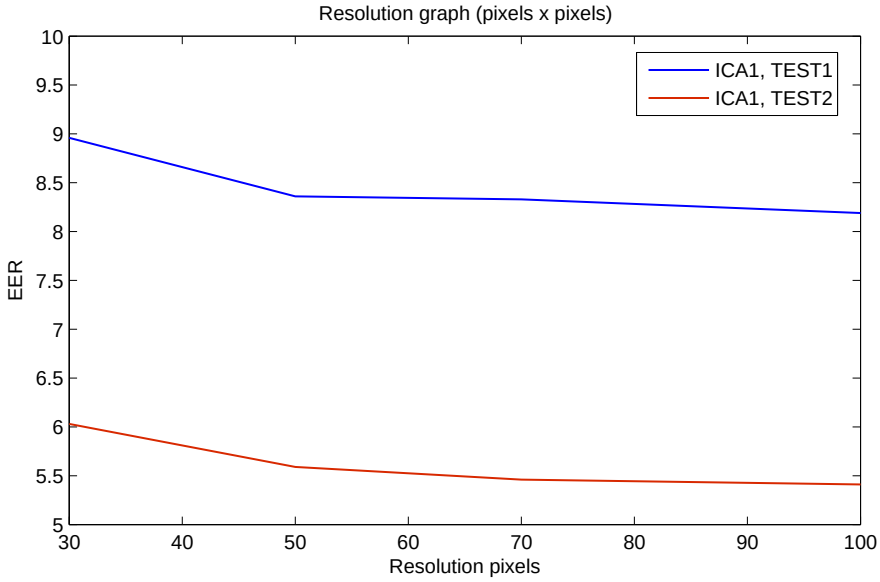

Figure 4.7. ICA1, EER performances for different resolutions (30×30, 50×50, 70×70 and 100×100)

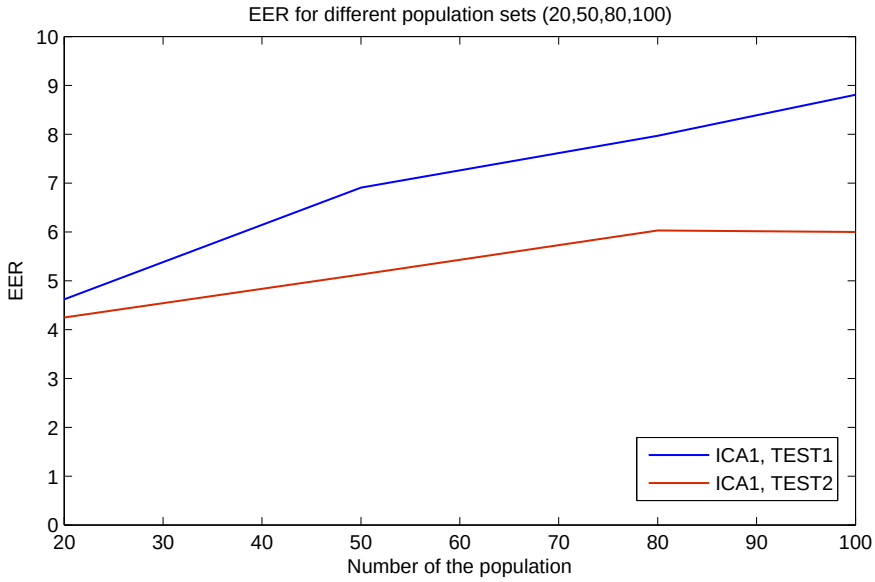

Figure 4.8. ICA1, EER performances for different population sizes (20, 50, 80, 100) for TEST1 and TEST2

4.3.6. Results for Time Lapse

Results of the two sets Version1 and Version2 that are collected at different times have been provided. There are small identification and EER differences between the versions. The results can be observed from Table 4.9.

Table 4.9. Results for the data taken in different times (TEST1 and TEST2)

Version		Version 1	Version 2
ICA1 (TEST1)	Iden.Rate:	96.00	81.33
	EER:	1.98	9.25
ICA1 (TEST2)	Iden.Rate:	98.66	88.00
	EER:	0.33	5.02

The experiments revealed that both appearance-based methods, ICA and NMF, outperform LEM, which is a geometry-based method. In the LEM method, as the veins become visible in the bag and activity, the identification rates increase. On the

other hand, for ice images, due to the veins becoming less visible, the identification and verification performances also decrease.

We use paired t-test to compare the accuracies for statistically significant difference. At a significance level % 5, the paired t-test confirmed that the algorithms are statistically different for individual test sets.

5. CONCLUSIONS

We have collected a near-infrared based hand vein database, acquired under adverse conditions mirroring real life situations and designed a new biometric identification system based on hand vein patterns. The novelty of the thesis is the joint consideration of appearance-based and geometry-based features. The appearance-based features are extracted using ICA and NMF algorithms, and they both have proved superior to the geometry-based LEM technique. Under normal conditions there is no advantage accruing to the verification rate from any classifier fusion. However their fusion turns out to be beneficial for hand vein biometry under stressed conditions. The major conclusions can be summarized as follows:

- Under stressed conditions, ICA architecture 2 is the best feature set.
- According to all results, ICA architecture 1 is always better then its competitors ICA2, LEM and NMF.
- For stressed conditions, such as strenuous exercise with the hand, there are large performance drops.
- Fusion of the classifier scores under sum rule improves the performance.

We have shown that hand vein pattern biometry is a promising technique. Our future research will address methods to make this biometric technique more robust in adverse conditions. Our database will be made open for the sake of reproducable results.

6. FUTURE DIRECTIONS FOR STUDY

There are several possible avenues to pursue hand vein-based biometry. These can be collected under the clusters of "Extensions of the Present Work"and "New Methods".

6.1. Extensions of the Present Work

First, we will attempt to reproduce the methods of other researchers and apply them on our database. This will allow for a more fair comparison among competing methods. Each method should have set its parameters at its optimum performance point and run on our database. Different aspects like scalability with gallery size, performance at different resolutions should be compared in a detailed way.

Second, we should obtain the intra-subject distance histograms (genuine-to-genuine) and compare them with inter-subject distance histograms (impostor-to-genuine). In addition, the right hand-to left hand vein pattern distance histograms would be of interest, and would indicate whether ambidextrous biometry is possible or not. For example, right hand identification performances and the identification performances of left hands on the enrolled right hands will be studied. Another future study will focus on the fusion of the left and right hand results.

Thirdly, the verification results should be illustrated with ROC: Receiver Operating Characteristic curves and the AuC figure, that is, the area under the ROC curve should be computed. Recall that AuC is equivalent to the theoretical maximum achievable correct rate of a binary classification problem. In this way, one can avoid measures like correct recognition, hit and false alarm rates which can sometimes be quite misleading since they depend on the operation threshold.

Fourth, the identification results should be illustrated with CMC: Cumulative

Match Count curves, and similarly, these curves can be reduced to a single number via calculation of the AuC.

6.2. New Methods

(i) Vessel extraction methods: There is no single best segmentation method to extract vessels under varying conditions. However, biomedical image research is replete with methods to extract vessel patterns. A sampling of methods that can potentially be used is listed in the references [29] to [30].

(ii) Singular points: We conjecture that the geometry of singular points, i.e., bifurcations and end points, contain relevant discriminative information. These are reminiscent of fingerprint biometrics, where the fingerprint pattern is well represented by the ridge endings and bifurcations and deltas. These critical points are commonly referred to as minutiae, and they are widely used to match a pair of fingerprints, and hence to identify a person [29]. For hand biometry, Wang et al. [31] used a similar set of minutiae points to represent the vein patterns. The branching points and the ending points in the vein pattern skeleton image were the two types of critical points to be extracted. We will investigate methods to combine appearance and/or skeleton information with the spatial distribution of singularities. Registration process may be applied after LEM construction or bifurcation and ending points of the hand vein regions may be used for image alignment.

(iii) Graph-based method for vessel extraction and recognition: Another approach on vessel tracking is the use of graph representations. The segmentation process is reduced to finding the optimum path in a graph representation of the image. The disadvantage of the vessel tracking approaches is that they are not fully automatic, i.e. they often require selection of the starting and end points. In [32] graph theory is used in order to track two edges concurently that constructs vessel contours in angiogram images. The position and size of section and the curvature of the segment are used in the formal structure model. The detection process employs a heuristic search method based on a uniform cost A* [33] algorithm. The best edge is found as the optimum path in a graph representation of the image. A similar

approach may be implemented and a graph representation of hand vein images may be extracted. On this content, polygonization of vein skeletons and as well as non-vein parts may be considered. Similar as fingerprint recognition, in vein recognition graph-based methods can be used to compare two vein patterns [30]. Using a graph based comparison will also remove the registration step; hence, the problems encountered during the registration process will be mitigated.

(iv) Foreground and background skeletons: In the present work, we have only used the skeleton of the foreground. Similarly, the skeleton of the complementary areas can be used separately or jointly with vessel skeletons for recognition.

(v) Shape spectrum: Shape spectrum is a good shape descriptor, especially for diffuse shape patterns as in the case of vein patterns. For example, one can use a morphological opening operation with increasingly larger structural element S(t). Then the ratio of the area of the for each size t between the resulting pattern and that of the original pattern can be calculated. The normalized size distribution is called the pattern spectrum and its derivative called the density function.

REFERENCES

1. Jain, A. K., A. Ross, and S. Prabhakar, "An Introduction to Biometric Recognition", *IEEE Transactions on Circuits and Systems for Video Technology, Special Issue on Image- and Video-Based Biometrics*, Vol. 14, No. 1, January 2004.

2. Jain, A. K., P. Flynn, and A. A. Ross, *Handbook of Biometrics*, Springer, 2008.

3. Lin, C.-L. and K.-C. Fan, "Biometric Verification Using Thermal Images of Palm-Dorsa Vein Patterns", *IEEE Trans. Circuits and Sys. For Video Technology*, Vol. 14, No. 2, pp. 199–213, February 2004.

4. Toh, K.-A., H.-L. Eng, Y.-S. Choo, Y.-L. Cha, W.-Y. Yau, and K.-S. Low, "Identity Verification Through Palm Vein and Crease Texture", *Lecture Notes in Computer Science*, 2005.

5. Wang, L.-Y., G. Leedham, and D. S.-Y. Cho, "Infrared Imaging of Hand Vein Patterns for Biometric Purposes", *The Institution of Engineering and Technology, Computer Vision*, Vol. 1, pp. 113–122, 2007.

6. Zhang, T. Y. and C. Y. Suen, "A Fast Parallel Algorithm for Thinning Digital Patterns", *Communications of the ACM*, Vol. 27, No. 3, pp. 236 – 239, March 1984.

7. Ding, Y., D. Zhuang, and K. Wang, "A Study of Hand Vein Recognition Method", *Proceedings of IEEE International Conference on Mechatronics and Automation*, 2005.

8. Wang, Z., B. Zhang, W. Chen, and Y. Gao, "A Performance Evaluation of Shape and Texture Based Methods for Vein Recognition", *Congress on Image and Signal Processing*, Vol. 2, pp. 659–661, 2008.

9. Wang, J.-G., W.-Y. Yau, and A. Suwandy, "Fusion of Palmprint and Palm Vein Images for Person Recognition Based on Laplacianpalm Feature", *Pattern Recognition*, Vol. 41, p. 15311544, May 2008.

10. Wang, L. and G. Leedham, "A Watershed Algorithmic Approach for Gray-Scale Skeletonization in Thermal Vein Pattern Biometrics", *Lecture Notes in Computer Science*, Vol. 4456, pp. 935–942, September 2007.

11. Carretero, O. A., "Vascular Remodeling and the Kallikrein-Kinin System", *J. Clin.Invest.*, Vol. 115, pp. 588–591, March 2005.

12. Carmeliet, P. and R. K. Jain, "Angiogenesis in Cancer and Other Diseases", *Nature*, Vol. 407, pp. 249–257, 2000.

13. Gray, H., *Anatomy of the Human Body*, Philadelphia: Lea and Febiger, 1918; Online Edition Bartleby.com, May 2000.

14. Fantini, S. and M. A. Franceschini, *Handbook of Optical Biomedical Diagnostics*, SPIE Press, Bellingham, WA, 2002.

15. Watec, "Specifications of the WAT-902H2 ULTIMATE Camera", June 2010, `http://www.watec.co.jp/english/bw/wat_902_ultimate.html`.

16. Wray, S., M. Cope, D. T. Delpy, J. S. Wyatt, E.Osmund, and R. Reynolds, "Characterization of the Near Infrared Absorption Spectra of Cytochrome aa3 and Hemoglobin for the Non-invasive Monitoring of Cerebral Oxygenation", *Biochimica et Biophysica Acta*, Vol. 933, No. 1, pp. 184–192, March 1988.

17. Konukoglu, E., E. Yoruk, J. Darbon, and B. Sankur, "Shape-Based Hand Recognition", *IEEE Transactions on Image Processing*, Vol. 15, No. 7, pp. 1803–1815, 2006.

18. Yoruk, E., H. Dutagaci, and B. Sankur, "Hand Biometry", *Image and Vision Computing*, Vol. 24, No. 5, pp. 483–497, 2006.

19. Weeks, A. R., *Fundamentals of Electronic Image Processing*, SPIE Press, 1996.

20. Sezgin, M. and B. Sankur, "Survey over Image Thresholding Techniques and Quantitative Performance Evaluation", *Journal of Electronic Imaging*, Vol. 13, No. 1, pp. 146–165, 2004.

21. Gonzalez, R. C., R. E. Woods, and S. L. Eddins, *Digital Image Processing Using Matlab*, Prentice Hall, 2004.

22. Bartlett, M. S., J. R. Movellan, and T. J. Sejnowski, "Face Recognition by Independent Component Analysis", *IEEE Transactions on Neural Networks*, Vol. 13, No. 6, November 2002.

23. Hyvrinen, A. and E. Oja, "Independent Component Analysis: Algorithms and Applications", *Neural Networks*, Vol. 13, No. 4-5, pp. 411–430, 2000.

24. Lee, D. D. and H. S. Seung, "Algorithms for Non-negative Matrix Factorization", *Advances in Neural Information Processing Systems*, Vol. 13, pp. 556–562, 2001.

25. Hoyer, P. O., "Non-negative Matrix Factorization with Sparseness Constraints", *Journal of Machine Learning Research*, Vol. 5, pp. 1457 – 1469, December 2004.

26. Gao, Y.-S. and M. K. H. Leung, "Line Segment Hausdorff Distance on Face Matching", *Pattern Recognition*, Vol. 35, No. 2, pp. 361–371, February 2002.

27. Gokberk, B., A. A. Salah, and L. Akarun, "Rank-Based Decision Fusion for 3D Shape-Based Face Recognition", *Audio- and Video-Based Biometric Person Authentication (AVBPA)*, July 2005.

28. Mansfield, A. J. and J. L. Wayman, "Best Practices in Testing and Reporting Performance of Biometric Devices, Version 2.01", *NPL Report CMSC 14/02*, August 2002.

29. Jain, A. K., L. Hong, S. Pankanti, and R. Bolle, "An Identity-Authentication

System Using Fingerprints", *Proc. IEEE*, Vol. 85, No. 9, pp. 1365–1388, September 1997.

30. Luo, H., F. Yu, J. Pan, S. Chu, and P. Tsai, "A Survey of Vein Recognition Techniques", *Information Technology Journal*, Vol. 9, No. 6, pp. 1142–1149, 2010.

31. Wang, L.-Y., G. Leedham, and D. S.-Y. Cho, "Minutiae Feature Analysis for Infrared Hand Vein Pattern Biometrics", *The Journal of the Pattern Recognition Society*, Vol. 41, No. 3, pp. 920–929, March 2008.

32. Lecornu, L., C. Roux, and J. Jacque, "Extraction of Vessel Contours in Angiograms by Simultaneous Tracking of the Two Edges", *IEEE Conf. Eng. in Medicine and Bio.*, Vol. 1, pp. 678–679, 1994.

33. Martelli, A., "An Application of Heuristic Search Methods to Edge and Contour Detection", *Comm. ACM*, Vol. 19, pp. 73–83, 1976.